

Perturbative and nonperturbative QCD corrections in polarized nucleon structure functions and spin asymmetries of nucleons

F. Zaidi,¹ M. Sajjad Athar*,¹ and S. K. Singh¹

¹*Department of Physics, Aligarh Muslim University, Aligarh - 202002, India*

We have studied the deep inelastic scattering of polarized charged leptons from polarized nucleon targets and evaluated the polarized structure functions $g_{1,2}(x, Q^2)$ for protons and neutrons as well as the nucleon asymmetries $A_{1p}(x, Q^2)$ and $A_{2p}(x, Q^2)$ for protons. The higher order perturbative corrections up to the next-to-next-to-the-leading order (NNLO) using the parameterization of LSS05 polarized parton distribution functions in the 3-flavor MSbar scheme and the nonperturbative corrections viz. the twist-3 corrections and target mass corrections (TMC) have been included in the calculations. The numerical results for the polarized nucleon structure functions and the proton asymmetries are presented and compared with the experimental results. The sum rule integrals of the nucleon structure functions corresponding to the Ellis-Jaffe, Bjorken, Gottfried and Burkhardt-Cottingham sum rules have been evaluated numerically and are compared with the experimental results.

PACS numbers: 13.15.+g, 13.60.Hb, 21.65.+f, 24.10.-i

I. INTRODUCTION

The study of nucleon spin physics is important in understanding the spin structure of the nucleon beyond the simple picture of nucleon spin being composed of the spins of three spin-1/2 valence quarks of the lightest flavors u and d in various quark models proposed for the structure of nucleon. It was realized that this simple picture of nucleon spin is not valid when the results from the pioneering experiments by European Muon Collaboration (EMC) at CERN on the spin structure function of proton i.e. $g_{1p}(x, Q^2)$ [1]; where x and Q^2 are the standard kinematic variables to describe the deep inelastic scattering (DIS) of the polarized muons on the polarized protons, were interpreted in the light of the predictions of the naive quark parton model (QPM) [2, 3] along with the results of the neutron and hyperon β decays analyzed assuming the $SU(3)$ symmetry. The interpretation of the quark parton model result of $g_{1p}(x, Q^2)$ done in a three flavor quark model using u , d and s quarks found that **(i)** the total spin contribution from quark spins to the proton spin is only a small fraction of the proton spin and **(ii)** the contribution from the strange quark sea is not negligible but large and negative. This surprising result, known as the “proton spin crisis” in literature, led to enormous experimental as well as theoretical interest in the study of the spin structure functions of the nucleons.

Experimentally extensive efforts have been made to make further measurements of the spin structure functions of the nucleon in the entire kinematic region of x and Q^2 in various experiments on the deep inelastic scattering done with the charged leptons at SLAC [4–9], CERN [10–15], DESY [16–18] and JLAB [19–23]. Theoretically, many attempts have been made to study the spin structure functions of the nucleon by including various corrections to the results obtained in the naive quark parton model (QPM) in order to resolve the “proton spin crisis” [24–29] using mathematical techniques, developed in quantum chromodynamics (QCD), to describe the strong interactions of quarks and gluons inside the nucleon. The various theoretical and experimental efforts to resolve the proton spin crisis have led to our present understanding that the total nucleon spin is composed of the contributions from the spins of quarks, gluons and their angular momenta inside the nucleon. Subsequently, the total spin of the nucleon S is, therefore, written (in units of \hbar) as:

$$S = \frac{1}{2} = \frac{1}{2}\Delta\Sigma + \Delta G + L, \quad (1)$$

where $\Delta\Sigma$ is the contribution of the quark spins, ΔG is the contribution of the gluons and $L = L_q + L_g$ is the contribution of the angular momenta of quarks (L_q) and gluon (L_g). In Eq. 1, $\Delta\Sigma = \sum_{q=u,d,s} \Delta q$ with $\Delta q = \int_0^1 (q^+(x) - q^-(x)) dx$, where $q^+(x)$ and $q^-(x)$ are the momentum distribution of the quarks plus antiquarks having spins parallel and anti-parallel to the direction of the nucleon spin. Therefore, $\frac{1}{2}\Delta\Sigma$ represents the spin contribution of the quarks spins to the spin of the nucleon. The latest experimental results from COMPASS [15] show that $\Delta\Sigma = 0.32 \pm 0.02(\text{stat}) \pm 0.04(\text{sys}) \pm 0.05(\text{evol})$ which are in agreement with the results from HERMES [17], showing that the quark spins contribute about 32% of the proton spin and the contribution from the strange quarks is quite

* Corresponding author: sajathar@gmail.com

substantial and negative thus confirming the earlier results from the EMC experiments leading to the proton spin crisis with better statistics.

The origin of the proton spin crisis lies in the interpretation of the spin structure function $g_{1p}(x, Q^2)$ obtained in the naive quark parton model (QPM) which needs to be improved by including various corrections to this result. In QPM, the spin structure function $g_{1p}(x)$ is independent of Q^2 and therefore the extraction of $\Delta\Sigma$ using the expression for $g_{1p}(x)$ i.e., $g_{1p}(x) = \frac{1}{2} \sum_{q=u,d,s} \epsilon_q^2 \Delta q(x)$ and the results of the SU(3) symmetric analysis of the neutron and the hyperon β -decays is independent of Q^2 . However, when various corrections to the $g_{1p}(x, Q^2)$ going beyond the QPM are calculated, the $\Delta\Sigma$ acquires a Q^2 dependence which is attributed to the presence of quark-quark and quark-gluon interactions in the nucleon. Moreover, ΔG and L also make Q^2 dependent contributions to the nucleon spin when these corrections are calculated. The separation of the nucleon spin into the contributions from the quarks and gluons pieces shown in Eq. 1, therefore, requires a consistent description of the strong interactions of the quarks and gluons inside the nucleon using current “state-of-the-art-methods” developed in the perturbative and nonperturbative QCD in order to calculate various corrections to the spin structure functions of nucleons beyond the results obtained in the naive quark parton model.

The differential cross section $\left(\frac{d^2\sigma^{UU}}{d\Omega' dE'}\right)$ for the scattering of unpolarized (U) electrons from the unpolarized (U) nucleons is expressed in terms of unpolarized nucleon structure functions $F_{1N}(x, Q^2)$ and $F_{2N}(x, Q^2)$ which are determined from the analysis of the unpolarized cross section $\frac{d^2\sigma^{UU}}{d\Omega' dE'}$. While the differential cross section for the scattering of polarized electron from the polarized nucleons involves two additional polarized nucleon structure functions $g_{1N}(x, Q^2)$ and $g_{2N}(x, Q^2)$ which are extracted from the measurement of the asymmetries in the scattering of longitudinally polarized electrons/muons from the longitudinally polarized nucleons, i.e., A_{\parallel} and from the transversely polarized nucleon, i.e., A_{\perp} , defined as

$$A_{\parallel} = \frac{\frac{d^2\sigma^{\uparrow\uparrow}}{d\Omega' dE'} - \frac{d^2\sigma^{\uparrow\downarrow}}{d\Omega' dE'}}{\frac{d^2\sigma^{\uparrow\uparrow}}{d\Omega' dE'} + \frac{d^2\sigma^{\uparrow\downarrow}}{d\Omega' dE'}}, \quad (2)$$

$$A_{\perp} = \frac{\frac{d^2\sigma^{\uparrow\Rightarrow}}{d\Omega' dE'} - \frac{d^2\sigma^{\uparrow\Leftarrow}}{d\Omega' dE'}}{\frac{d^2\sigma^{\uparrow\Rightarrow}}{d\Omega' dE'} + \frac{d^2\sigma^{\uparrow\Leftarrow}}{d\Omega' dE'}}, \quad (3)$$

where the symbols $(\uparrow\downarrow) \uparrow\uparrow$ correspond to the (anti)parallel spin configuration of the longitudinally polarized nucleon (\uparrow or \downarrow) with the polarization of the incoming lepton beam (\uparrow), and $(\uparrow\Rightarrow) \uparrow\Leftarrow$ correspond to the case of a nucleon polarized transversely (with opposite helicities) to the direction of the lepton beam. These nucleon asymmetries are expressed in terms of the nucleon asymmetries $A_1(x, Q^2)$ and $A_2(x, Q^2)$ defined in the case of the virtual photon-nucleon scattering which are given directly in terms of the polarized structure functions $g_{1N}(x, Q^2)$ and $g_{2N}(x, Q^2)$ through some kinematic factors involving the energy (E') and the scattering angle (θ) of the final state lepton as discussed in section II. Therefore, an experimental extraction of $A_1(x, Q^2)$ and $A_2(x, Q^2)$ from the observed cross sections in the scattering of longitudinally polarized electrons from the longitudinally and transversely polarized nucleons determines the x and Q^2 dependence of the polarized structure functions $g_{1N}(x, Q^2)$ and $g_{2N}(x, Q^2)$.

Theoretically, the structure functions $F_{1N}(x, Q^2)$, $F_{2N}(x, Q^2)$, $g_{1N}(x, Q^2)$, $g_{2N}(x, Q^2)$, and the spin asymmetries $A_{1N}(x, Q^2)$ and $A_{2N}(x, Q^2)$ for the nucleons $N = p, n$ are calculated from a model used to describe the deep inelastic scattering of charged leptons from nucleons. Historically, the simplest model proposed by Feynman [2, 3], i.e. the quark-parton model has been used to describe the DIS of the charged leptons from the nucleons. In this model the DIS of the charged leptons from the nucleon is viewed as an incoherent sum of elastic scattering processes of the charged leptons from the individual constituents of the nucleon called partons (charged partons in case of the quark constituents) which are assumed to be point like, free i.e. non-interacting with neighboring partons in the asymptotic limit of the kinematic variables Q^2 and ν , i.e., $Q^2 \rightarrow \infty$, $\nu \rightarrow \infty$, with $\frac{Q^2}{2M\nu} = x$, in which the quarks-partons are also treated as massless. This assumption is reasonable in this kinematic region due to the asymptotic freedom of QCD in describing the strong interactions of quarks and gluons. In the naive quark parton model, the nucleon structure functions are predicted to scale, i.e., they depend only upon one variable, i.e., $x \left(= \frac{Q^2}{2M\nu} \right)$ and are independent of Q^2 . This is called Bjorken scaling [30], a phenomenon which is experimentally confirmed in many measurements of the structure functions reported from the various DIS experiments albeit with a mild Q^2 dependence [31–34]. The mild Q^2 dependence seen in the structure functions in the realistic conditions of the DIS experiments where Q^2 and ν are very high but still finite implies that quark partons are not completely free but are interacting with other quark partons through gluon exchange as envisaged in the QCD picture of the nucleon. Inclusion of this interaction in the kinematic region of high but non-asymptotic Q^2 region introduces some Q^2 dependence in the nucleon structure functions. Moreover, the gluons themselves are self interacting inside the nucleon which also contribute to the nucleon structure functions with a Q^2 dependence. The corrections to the nucleon structure functions due to the interactions

of quark partons through the exchange of gluons and self interaction of gluons inside the nucleon are calculated using the methods of perturbative QCD treating it in increasing orders of strong coupling α_s of the quarks and gluons interactions generally, labeled as the leading order (LO), next-to-leading order (NLO), next-to-next-to-leading order (NNLO) depending on the higher order terms in the perturbative QCD. The theoretical formulation for calculating these corrections is based on the DGLAP evolution equations of QCD [35] which describes the Q^2 evolution of the nucleon structure functions as one moves towards lower Q^2 from the asymptotic limits of $Q^2 \rightarrow \infty$ [30]. These are called higher order perturbative corrections. In addition, there are nonperturbative corrections such as target mass corrections (TMC) which is related to the finite mass of the target nucleon and results in the modification of scattering kinematics, and the corrections arising due to the contribution of higher twist (HT) terms like twist-3, twist-4, etc., in the operator product expansion (OPE) of the hadronic tensor which describe the effect of parton (quark and gluon) correlations beyond the twist-2 operators in the calculation of nucleon structure functions [36–38]. These nonperturbative effects are significant in the kinematic region of high x and moderate Q^2 .

In the literature, various theoretical groups like the groups of Borsa et al. [39], Amiri et al. [40], Khanpour et al. [41], Mirjalili et al. [42], Blumlein et al. [43], Leader et al. [44], etc. have phenomenologically determined the polarized nucleon structure functions using the experimental data. For example, Mirjalili et al. [42] have evaluated the spin structure functions $g_{1N}(x, Q^2)$ and $g_{2N}(x, Q^2)$ by analyzing the updated world data up to NNLO using Jacobi polynomials expansion approach. Moreover, they have included the TMC effect following Ref. [45] and higher-twist corrections following the BLMP model [46] in which nucleon structure function are fitted phenomenologically. Leader et al. [44] have reported the polarized parton density distribution functions (PPDFs) determined phenomenologically up to NLO in both the JET and MSbar factorization schemes using the inclusive DIS world data. A comparison of polarized parton density distribution functions using different phenomenological parameterizations which are acronym as BB [43], KATAO [47], DSSV [48], AAC09 [49], TKA [50], NNPDF [51] is shown in Ref. [41] and a model dependence has been observed in the wide range of Bjorken x .

In this work we focus on the theoretical calculation for unpolarized and polarized structure functions by including the higher order perturbative and nonperturbative QCD corrections to the QPM results. Using the structure functions $F_{1p,2p}(x, Q^2)$, $F_{1n,2n}(x, Q^2)$, $g_{1p,2p}(x, Q^2)$, $g_{1n,2n}(x, Q^2)$, proton asymmetries $A_{1p,2p}(x, Q^2)$, and various sum rule integrals corresponding to Ellis-Jaffe, Bjorken, Gottfried and Burkhardt-Cottingham have been evaluated. In case of the polarized structure functions $g_{1p,2p}(x, Q^2)$ and $g_{1n,2n}(x, Q^2)$, the higher order perturbative corrections up to NNLO, the nonperturbative corrections from twist-3 operators and the target mass corrections have been included in a 3-quark flavors MSbar scheme [45, 52–54]. In case of the unpolarized structure functions $F_{1p,2p}(x, Q^2)$ the results have been taken from our earlier work [55] which includes the corrections due to the higher order perturbative evolution of the parton densities up to NNLO, and the nonperturbative target mass corrections in order to calculate the proton asymmetries $A_{1p,2p}(x, Q^2)$.

In section II, we describe the formalism for calculating the differential cross sections, nucleon asymmetries and write various sum rules in terms of the nucleon structure functions which are discussed in section III in the QPM, where the methods to calculate the nonperturbative and perturbative corrections are also discussed. In section IV, we present the numerical results for $F_{1p,2p}(x, Q^2)$, $F_{1n,2n}(x, Q^2)$, $g_{1p,2p}(x, Q^2)$, $g_{1n,2n}(x, Q^2)$, $A_{1p,2p}(x, Q^2)$ and different sum rule integrals and compare them with the available experimental results. In section V, we give a brief summary and conclusion of our work.

II. FORMALISM

A. Cross sections

The differential scattering cross section for the longitudinally polarized lepton induced DIS off a polarized nucleon target is given by [25, 56]

$$\frac{d^2\sigma}{d\Omega' dE'} = \frac{4\alpha^2}{Q^4} \frac{|\vec{k}'|}{|\vec{k}|} L_{\mu\nu} W_N^{\mu\nu}, \quad (4)$$

where \vec{k} and \vec{k}' are respectively the three momenta of the initial and final state leptons, α is the fine structure constant, E' is the outgoing lepton energy, Ω' is the solid angle for detecting the final state lepton in the lab frame and virtuality $Q^2 = -q^2$ with $q^\mu = (k^\mu - k'^\mu)$. In the above expression, $L_{\mu\nu}$ is the leptonic tensor for the polarized lepton beam

given by [56]:

$$\begin{aligned} L_{\mu\nu} &= L_{\mu\nu}^{(S)} + L_{\mu\nu}^{(A)}, \\ L_{\mu\nu}^{(S)} &= k_\mu k'_\nu + k'_\mu k_\nu - (k \cdot k' - m_l^2) g_{\mu\nu} \\ L_{\mu\nu}^{(A)} &= i m_l \epsilon_{\mu\nu\alpha\beta} s_l^\alpha q^\beta \end{aligned} \quad (5)$$

and summation is performed over the polarization of the final state lepton. In the above expression m_l is the charged lepton mass, $L_{\mu\nu}^{(S)}$ corresponds to the symmetric part of the leptonic tensor, and $L_{\mu\nu}^{(A)}$ corresponds to the anti-symmetric part which appears due to the spin contribution of polarized lepton beam. We have considered the longitudinally polarized lepton beam with spin 4-vector s_l^μ defined as

$$s_l^\mu = \left(\frac{\vec{k}}{m_l}, 0, 0, \frac{E}{m_l} \right), \quad (6)$$

where E is the energy of incoming lepton beam. We express the nucleon hadronic tensor $W_N^{\mu\nu}$ as a sum of symmetric and anti-symmetric tensors $W_{N,(S)}^{\mu\nu}$ and $W_{N,(A)}^{\mu\nu}$ (in Eq. 4) in terms of the scalar functions $W_{iN}(\nu, Q^2)$ and $G_{iN}(\nu, Q^2)$, ($i = 1 - 2$) as [25, 56]:

$$W_N^{\mu\nu} = W_{N,(S)}^{\mu\nu} + W_{N,(A)}^{\mu\nu} \quad (7)$$

which are written as

$$W_{N,(S)}^{\mu\nu} = \left(-g^{\mu\nu} + \frac{q^\mu q^\nu}{q^2} \right) W_{1N}(\nu, Q^2) + \left(p^\mu - \frac{p \cdot q}{q^2} q^\mu \right) \left(p^\nu - \frac{p \cdot q}{q^2} q^\nu \right) \frac{W_{2N}(\nu, Q^2)}{M^2} \quad (8)$$

$$W_{N,(A)}^{\mu\nu} = i \epsilon^{\mu\nu\rho\sigma} q_\rho s_{N\sigma} M G_{1N}(\nu, Q^2) + i \epsilon^{\mu\nu\rho\sigma} q_\rho (p \cdot q s_{N\sigma} - s_N \cdot q p_\sigma) \frac{G_{2N}(\nu, Q^2)}{M}, \quad (9)$$

with $\nu (= E - E')$ is the energy transferred to the nucleon target by the lepton, $p^\mu = (0, 0, 0, M)$ is the four momentum of the target nucleon which is considered to be at rest in the laboratory frame and M is the target nucleon mass. $s_N^\mu = (0, \hat{s}_N)$ is the proton spin 4-vector. For the case of longitudinally polarized spin 4-vector $s_{N,L}^\mu$:

$$s_{N,L}^\mu = \begin{cases} (0, 0, 0, 1); & \text{for } \lambda_N = +1 \\ (0, 0, 0, -1); & \text{for } \lambda_N = -1 \end{cases}, \quad (10)$$

where λ_N is the helicity of the target nucleon. When nucleon is considered to have transverse polarization, i.e. with a spin orthogonal to the lepton direction (z-axis here, $k^\mu = (E, 0, 0, |\vec{k}|)$) at an angle α to the x -axis, the components of spin are:

$$s_{N,T}^\mu = (0, \cos \alpha, \sin \alpha, 0) \quad (11)$$

In the present work, we have considered the case of longitudinally polarized nucleon target only. After performing some algebra to calculate $L_{\mu\nu} W_N^{\mu\nu}$ using Eq. 5-10, one obtains the differential cross sections in terms of the nucleon structure functions:

$$\frac{d^2\sigma^{\uparrow\downarrow}}{d\Omega' dE'} + \frac{d^2\sigma^{\uparrow\uparrow}}{d\Omega' dE'} = \frac{8\alpha^2 E'^2}{Q^4} \left[\cos^2\left(\frac{\theta}{2}\right) W_{2N}(\nu, Q^2) + 2\sin^2\left(\frac{\theta}{2}\right) W_{1N}(\nu, Q^2) \right] \quad (12)$$

and

$$\frac{d^2\sigma^{\uparrow\downarrow}}{d\Omega' dE'} - \frac{d^2\sigma^{\uparrow\uparrow}}{d\Omega' dE'} = \frac{4\alpha^2}{Q^2} \frac{E'}{E} \left[M(E + E' \cos\theta) G_{1N}(\nu, Q^2) - Q^2 G_{2N}(\nu, Q^2) \right], \quad (13)$$

where θ is the lepton scattering angle. These nucleon structure functions are in turn expressed in terms of the dimensionless nucleon structure functions ($F_{iN}(x)$ and $g_{iN}(x)$; ($i = 1, 2$)) using the following relations [25, 56]:

$$W_{1N}(\nu, Q^2) = \frac{F_{1N}(x)}{M}, \quad W_{2N}(\nu, Q^2) = \frac{F_{2N}(x)}{\nu}, \quad (14)$$

$$G_{1N}(\nu, Q^2) = \frac{g_{1N}(x)}{M^2 \nu}, \quad G_{2N}(\nu, Q^2) = \frac{g_{2N}(x)}{M \nu^2}. \quad (15)$$

Using the above relations in Eq. 13, one obtains the expression of the differential cross section for the deep inelastic scattering of a longitudinally polarized charged lepton from a longitudinally polarized nucleon which is expressed in terms of the two structure functions $g_{1N}(x, Q^2)$ and $g_{2N}(x, Q^2)$ as:

$$\frac{d^2\sigma^{\uparrow\downarrow}}{d\Omega' dE'} - \frac{d^2\sigma^{\uparrow\uparrow}}{d\Omega' dE'} = \frac{4\alpha^2}{Q^2} \frac{E'}{E} \frac{1}{M\nu} \left[(E + E' \cos\theta)g_{1N}(x, Q^2) - \frac{Q^2}{\nu} g_{2N}(x, Q^2) \right], \quad (16)$$

The polarized structure function $g_{1N}(x, Q^2)$ provides information about the longitudinal polarization of the nucleon while the transverse polarization is described by $g_{1N}(x, Q^2) + g_{2N}(x, Q^2)$. The sum of differential cross sections with parallel and antiparallel spin configurations of target nucleon with lepton beam (Eq. 12) is twice of the differential cross section for the deep inelastic scattering of unpolarized charged leptons from unpolarized nucleons and is expressed in terms of the structure functions $F_{1N}(x, Q^2)$ and $F_{2N}(x, Q^2)$ as:

$$\frac{d^2\sigma^{UU}}{d\Omega' dE'} = \frac{4\alpha^2 E'^2}{Q^4 M\nu} \left[M \cos^2\left(\frac{\theta}{2}\right) F_{2N}(x) + 2\nu \sin^2\left(\frac{\theta}{2}\right) F_{1N}(x) \right], \quad (17)$$

The unpolarized dimensionless nucleon structure functions have already been discussed in our earlier works [55]. Therefore, in the present work, we will only discuss the formalism for the polarized nucleon structure functions.

B. Spin asymmetries

In general, the polarized nucleon structure functions are experimentally extracted from the spin asymmetries measurements. A longitudinally polarized lepton beam is scattered either from a longitudinally or transversely polarized nucleon target and therefore there are longitudinal (A_{\parallel}) as well as transverse (A_{\perp}) asymmetries [25, 56, 57]. Using these asymmetries, polarized nucleon structure functions $g_{1N,2N}(x, Q^2)$ are determined as follows:

$$g_{1N}(x, Q^2) = \frac{F_{1N}(x, Q^2)}{d'} \left[A_{\parallel} + \tan\left(\frac{\theta}{2}\right) A_{\perp} \right], \quad (18)$$

$$g_{2N}(x, Q^2) = \frac{y F_{1N}(x, Q^2)}{2d'} \left[\left(\frac{E}{E'} \operatorname{cosec}\theta + \cot\theta \right) A_{\perp} - A_{\parallel} \right], \quad (19)$$

where $d' = \frac{(1-\epsilon)(2-y)}{y(1+\epsilon R)}$, $y = \frac{\nu}{E}$, $\epsilon = \left(1 + 2(1 + \frac{1}{\gamma^2}) \tan^2(\theta/2)\right)^{-1}$, $\gamma^2 = \frac{Q^2}{\nu^2} = \frac{4M^2 x^2}{Q^2}$ and $R = \frac{(1+\gamma^2)F_{2N}(x, Q^2) - 2x F_{1N}(x, Q^2)}{2x F_{1N}(x, Q^2)}$. The kinematic variables E , E' , θ and Q^2 have already been defined earlier in the text.

A_{\parallel} and A_{\perp} are related to the virtual photon-nucleon asymmetries $A_1(x, Q^2)$ and $A_2(x, Q^2)$ which are defined as [5, 56]:

$$A_1 = \frac{d\sigma_{1/2} - d\sigma_{3/2}}{d\sigma_{1/2} + d\sigma_{3/2}} = \frac{1}{(1 + \eta\zeta)} \left(\frac{A_{\parallel}}{D} - \frac{\eta A_{\perp}}{d} \right), \quad (20)$$

$$A_2 = \frac{2d\sigma_{LT}}{d\sigma_{1/2} + d\sigma_{3/2}} = \frac{1}{(1 + \eta\zeta)} \left(\frac{\zeta A_{\parallel}}{D} + \frac{A_{\perp}}{d} \right), \quad (21)$$

where the kinematical factors are $d = D \sqrt{\frac{2\epsilon}{1+\epsilon}}$, $\eta = \frac{\epsilon\sqrt{Q^2}}{E - \epsilon E'}$, $\zeta = \frac{\eta(1+\epsilon)}{2\epsilon}$, and the photon depolarization factor $D = \left(1 - \frac{\epsilon E'}{E}\right) \frac{1}{(1+\epsilon R)}$. In the above expression, $(d\sigma_{1/2})d\sigma_{3/2}$ is the absorption cross section of a transversely polarized photon with spin polarized (anti)parallel to the spin of the longitudinally polarized nucleon, and $d\sigma_{LT}$ represents the interference term between the transversely and longitudinally polarized photon-nucleon amplitudes. These absorption cross sections are related to the nucleon structure functions as follows [58]:

$$d\sigma_{3/2} = \frac{4\pi\alpha^2}{M\sqrt{\nu^2 + Q^2}} \left(F_{1N}(x, Q^2) - g_{1N}(x, Q^2) + \frac{Q^2}{\nu^2} g_{2N}(x, Q^2) \right), \quad (22)$$

$$d\sigma_{1/2} = \frac{4\pi\alpha^2}{M\sqrt{\nu^2 + Q^2}} \left(F_{1N}(x, Q^2) + g_{1N}(x, Q^2) - \frac{Q^2}{\nu^2} g_{2N}(x, Q^2) \right), \quad (23)$$

$$d\sigma_{LT} = \frac{4\pi\alpha^2}{M\sqrt{\nu^2 + Q^2}} \sqrt{\left(\frac{Q^2}{\nu^2}\right)} \left(g_{1N}(x, Q^2) + g_{2N}(x, Q^2) \right). \quad (24)$$

Using Eqs. 18-21, we obtain [25, 56, 58]:

$$A_{\parallel} = D(A_1 + \eta A_2), \quad A_{\perp} = d(A_2 - \zeta A_1) \quad (25)$$

After some simplification, asymmetries are obtained in terms of the polarized and unpolarized nucleon structure functions as:

$$A_1 = \frac{g_{1N}(x, Q^2) - \gamma^2 g_{2N}(x, Q^2)}{F_{1N}(x, Q^2)}, \quad (26)$$

$$A_2 = \frac{\gamma (g_{1N}(x, Q^2) + g_{2N}(x, Q^2))}{F_{1N}(x, Q^2)}. \quad (27)$$

In the QPM corresponding to the asymptotic limit of Bjorken scaling, i.e., $Q^2 \rightarrow \infty$, $\nu \rightarrow \infty$, in which the asymmetries $A_1(x, Q^2)$ and $A_2(x, Q^2)$ are simplified, and $A_1(x, Q^2)$ and $A_2(x, Q^2)$ are given by

$$A_1(x, Q^2) = \frac{g_{1N}(x, Q^2)}{F_{1N}(x, Q^2)}, \quad A_2(x, Q^2) \rightarrow 0.$$

C. Study of sum rule integrals

There are various sum rules involving the nucleon structure functions $F_{2p,2n}(x, Q^2)$, $g_{1p,1n}(x, Q^2)$ and $g_{2p,2n}(x, Q^2)$ integrated over the entire kinematic region of x , i.e., $0 \leq x \leq 1$ for a given Q^2 . The sum rule integrals defined as $\int_0^1 F_{2p,2n}(x, Q^2) dx$, $\int_0^1 g_{1p,1n}(x, Q^2) dx$, $\int_0^1 g_{2p,2n}(x, Q^2) dx$ are given in terms of some physically observable quantities which can be measured in other processes. The numerical values of the sum rule integrals evaluated in various theoretical models for calculating the nucleon structure functions can be compared with experimental values of these integrals obtained in various experiments. However, the experimental values of the sum rule integrals have limitations as the experiments do not cover the entire kinematic range of x , i.e., $0 \leq x \leq 1$. In some cases the sum rule integrals are either quoted for the actual range of x_{min} and x_{max} considered in the experiment or an extrapolation is made to obtain the values of the nucleon structure functions in the lower as well as in the upper range of x not covered by the experiment. In the earlier case some uncertainties and model dependence due to the extrapolation procedure appears in the quoted values of the sum rule integrals. In this section, we describe the sum rules given by Gottfried, Bjorken, Ellis-Jaffe and Burkhardt-Cottingham. In the naive quark parton model, in which $Q^2 \rightarrow \infty$, $\nu \rightarrow \infty$ all the nucleon structure functions are independent of Q^2 , and these sum rules are given as:

(i) **Gottfried sum rule:** The Gottfried sum rule, also known as the valence isospin sum rule, is derived for the unpolarized structure function $F_2(x)$ of the proton and neutron and is given by [59]

$$S_G = \int_0^1 \frac{dx}{x} [F_{2p}(x) - F_{2n}(x)] = \frac{1}{3} \int_0^1 dx (u_v(x) - d_v(x)) + \frac{2}{3} \int_0^1 dx (\bar{u}(x) - \bar{d}(x)), \quad (28)$$

where $u_v(x)$ and $d_v(x)$ correspond to the valence up and valence down quarks densities. This sum rule is important to understand the momentum distribution of valence and sea quarks which are basically studied by comparing the proton and neutron structure functions. This may provide information about the possible existence of flavor asymmetry in the nucleon sea for the light quarks/antiquarks. In the case of SU(2) symmetric sea, the last term on the r.h.s. of Eq. 28 vanishes, which leads to:

$$S_G = \int_0^1 \frac{dx}{x} [F_2^p(x) - F_2^n(x)] = \frac{1}{3}. \quad (29)$$

(ii) **Bjorken sum rule:** Bjorken proposed a sum rule by taking the difference of proton and neutron first moments which was evaluated in the limit of very high Q^2 by using the techniques of Gell-Mann's current algebra [60–62] and isospin invariance. The Bjorken sum rule is given in terms of the integrals Γ_1^p and Γ_1^n [63, 64] as:

$$\Gamma_{1p} - \Gamma_{1n} = \int_0^1 dx g_{1p}(x) - \int_0^1 dx g_{1n}(x). \quad (30)$$

The integrals for proton and neutron polarized structure functions are given by

$$\Gamma_{1p} = \int_x^1 dx g_1^p(x) = \frac{1}{36} (a_8 + 3a_3 + 4a_0), \quad \Gamma_{1n} = \int_x^1 dx g_1^n(x) = \frac{1}{36} (a_8 - 3a_3 + 4a_0) \quad (31)$$

with

$$a_0 = \int_0^1 \Delta\Sigma(x) dx = \int_0^1 dx \left[\Delta u(x) + \Delta \bar{u}(x) + \Delta d(x) + \Delta \bar{d}(x) + \Delta s(x) + \Delta \bar{s}(x) \right], \quad (32)$$

$$a_3 = \int_0^1 dx \left[\Delta u(x) + \Delta \bar{u}(x) - \Delta d(x) - \Delta \bar{d}(x) \right], \quad (33)$$

$$a_8 = \int_0^1 dx \left[\Delta u(x) + \Delta \bar{u}(x) + \Delta d(x) + \Delta \bar{d}(x) - 2\Delta s(x) - 2\Delta \bar{s}(x) \right], \quad (34)$$

where a_0 is the singlet, and a_3 and a_8 are the non-singlet contributions to the polarized nucleon structure function $g_{1N}(x)$. The flavor non-singlet combinations are related to the β -decay parameters F and D of the baryon octet, i.e., $a_8 = 3F - D$ and $a_3 = F + D = |\frac{g_A}{g_V}|$, where g_A and g_V are the axial and vector coupling constants of neutron β -decay. Hence, in the limit of very high Q^2 , the Bjorken sum rule relates the ratio of axial to vector coupling constants:

$$S_{Bj} = \int_0^1 dx g_{1p}(x) - \int_0^1 dx g_{1n}(x) = \frac{a_3}{6} = \frac{1}{6} \left| \frac{g_A}{g_V} \right|. \quad (35)$$

However, for the moderate values of Q^2 perturbative QCD corrections come into the picture through the non-singlet parton coefficient functions containing the series expansion of strong coupling constant $\alpha_s(Q^2)$, and the sum rule is modified as:

$$S_{Bj} = \int_0^1 dx g_{1p}(x, Q^2) - \int_0^1 dx g_{1n}(x, Q^2) = \frac{1}{6} \left| \frac{g_A}{g_V} \right| \Delta C_{NS}(Q^2), \quad (36)$$

where $\Delta C_{NS}(Q^2)$ is the non-singlet polarized parton coefficient function which is discussed in section III B 1.

(iii) **Ellis-Jaffe sum rule:** Using the SU(3) symmetry along with the assumption of neglecting the polarizations of sea quarks, following sum rule was obtained by Ellis and Jaffe [65] in the QPM independently for protons and neutrons:

$$\left. \begin{aligned} S_{EJ}^p &= \int_0^1 dx g_{1p}(x) = \frac{1}{12} \left| \frac{g_A}{g_V} \right| \left[1 + \frac{5}{3} \left(\frac{3F-D}{F+D} \right) \right], \\ S_{EJ}^n &= \int_0^1 dx g_{1n}(x) = \frac{1}{12} \left| \frac{g_A}{g_V} \right| \left[-1 + \frac{5}{3} \left(\frac{3F-D}{F+D} \right) \right]. \end{aligned} \right\} \quad (37)$$

This is derived using Eqs. 31-34 which reduces to $a_0 = a_8 = 3F - D$ under the assumption that $\Delta s = 0 = \Delta \bar{q}$.

(iv) **Burkhardt-Cottingham sum rule:** Burkhardt-Cottingham sum rule is derived for the polarized spin structure function $g_{2N}(x)$ given by [66]:

$$\int_0^1 g_{2N}(x) dx = 0; \quad N = p, n \quad (38)$$

from the virtual Compton scattering dispersion relations in the limit of high Q^2 . This sum rule is obtained by considering the Wandzura-Wilczek relation [67] incorporating the twist-2 contribution.

When the various corrections to the nucleon structure functions are included, then the left hand side develops a Q^2 dependence which corresponds to the realistic experimental situations in which Q^2 is large but finite. In this case, the right hand side is modified by factors depending upon Q^2 which are different for the singlet and non-singlet combinations of quark helicity distributions Δu , Δd and Δs .

In the present work, we mainly calculate the sum rule integrals defined in the left hand side of various sum rules and compare them with the experimentally available values quoted in the kinematic regions of x corresponding to the experiments.

III. NUCLEON STRUCTURE FUNCTIONS

A. Quark Parton Model (QPM)

In QPM, the unpolarized structure functions $F_{2N}(x, Q^2)$ is given by [55, 68]:

$$F_{2N}(x) = x \sum_{i=1}^{n_f} e_i^2 q_i(x), \quad (39)$$

where n_f is the number of quark flavors, e_i is the charge of the corresponding quark, the sum over i extends over all flavors of quarks and antiquarks in the nucleon, and $q_i(x) = q^+(x) + q^-(x)$ with $q^+(x)$ and $q^-(x)$ as the quarks plus antiquarks momentum distribution having spin parallel and antiparallel to the nucleon spin. $q(x)$ represents the parton distribution functions (PDFs) which describes the probability of finding a quark/antiquark of flavor i carrying a momentum fraction x of the nucleon's momentum. The structure function $F_{1N}(x)$ is related with $F_{2N}(x)$ through the Callan-Gross relation [69], in the Bjorken limit, given by

$$F_{2N}(x) = 2x F_{1N}(x) \quad (40)$$

This gives

$$F_{2p}(x) = x \left[\frac{4}{9} (u(x) + \bar{u}(x)) + \frac{1}{9} (d(x) + \bar{d}(x)) + \frac{1}{9} (s(x) + \bar{s}(x)) \right] \quad (41)$$

$$F_{2n}(x) = x \left[\frac{1}{9} (u(x) + \bar{u}(x)) + \frac{4}{9} (d(x) + \bar{d}(x)) + \frac{1}{9} (s(x) + \bar{s}(x)) \right] \quad (42)$$

Similarly the polarized structure functions $g_{1N}(x)$ and $g_{2N}(x)$ are given as [52]:

$$g_{1N}(x) = \frac{1}{2} \sum_{i=1}^{n_f} e_i^2 (\Delta q_i(x)), \quad (43)$$

$$g_{2N}(x) = 0, \quad (44)$$

where $\Delta q_i(x) = q^+(x) - q^-(x)$.

At the lowest order, the polarized structure function for a proton target ($g_{1p}(x)$) is written in terms of the polarized parton density distribution functions as

$$g_{1p}(x) = \frac{1}{2} \left[\frac{4}{9} (\Delta u(x) + \Delta \bar{u}(x)) + \frac{1}{9} (\Delta d(x) + \Delta \bar{d}(x)) + \frac{1}{9} (\Delta s(x) + \Delta \bar{s}(x)) \right] \quad (45)$$

For a polarized neutron target, we use the isospin invariance and following Eq. 45 obtains:

$$g_{1n}(x) = \frac{1}{2} \left[\frac{1}{9} (\Delta u(x) + \Delta \bar{u}(x)) + \frac{4}{9} (\Delta d(x) + \Delta \bar{d}(x)) + \frac{1}{9} (\Delta s(x) + \Delta \bar{s}(x)) \right] \quad (46)$$

For an isoscalar nucleon target,

$$g_{iN}(x) = \frac{g_{ip}(x) + g_{in}(x)}{2}; \quad F_{iN}(x) = \frac{F_{ip}(x) + F_{in}(x)}{2}, \quad i = 1 - 2 \quad (47)$$

B. Corrections to QPM

1. Higher order perturbative corrections

It should be noted that in the naive QPM, $g_1(x)$ is independent of Q^2 . However, beyond the leading order there is an additional contribution from different sub processes such as $\gamma^* - q(\bar{q})$, $\gamma^* - g$ interactions to the parton coefficient functions. Due to the gluonic emission, polarized nucleon structure functions show Q^2 dependence, and the Q^2 evolution is performed by using the DGLAP evolution equations [35].

The general expression for the polarized structure function $g_{iN}(x)$, $i = 1 - 2$ in terms of the coefficient function (ΔC_f) convoluted over the polarized parton density distribution functions (PPDFs) Δf is given by [52, 53]:

$$g_{iN}(x) = \sum_{f=q,g} \Delta C_{f,i}^{(n)}(x) \otimes \Delta f(x), \quad i = 1 - 2, \quad (48)$$

where $n = 0, 1, 2, \dots$ and \otimes represents the Mellin convolution such that:

$$\Delta C_{f,i}(x) \otimes \Delta f(x) = \int_x^1 \Delta C_{f,i}(y) \Delta f\left(\frac{x}{y}\right) \frac{dy}{y}$$

Hence the polarized structure function at $N^{(n)}LO$; ($n = 1, 2, \dots$) is given by [52]:

$$\begin{aligned} g_{1N}(x, Q^2) &= \frac{1}{2} \int_x^1 \frac{dy}{y} \left[\frac{1}{n_f} \sum_{j=1}^{n_f} e_j^2 \left\{ \Delta\Sigma\left(\frac{x}{y}, \mu^2\right) \Delta C_q^{S,(n)}\left(y, \frac{Q^2}{\mu^2}\right) + \Delta G\left(\frac{x}{y}, \mu^2\right) \Delta C_g^{(n)}\left(y, \frac{Q^2}{\mu^2}\right) \right\} \right. \\ &\quad \left. + \Delta^{NS}\left(\frac{x}{y}, \mu^2\right) \Delta C_q^{NS,(n)}\left(y, \frac{Q^2}{\mu^2}\right) \right]. \end{aligned} \quad (49)$$

The other polarized structure function $g_2(x, Q^2)$ at the leading twist is given by the Wandzura-Wilczek (WW) relation [67]

$$g_{2N}^{WW}(x, Q^2) = -g_{1N}(x, Q^2) + \int_x^1 g_{1N}(y, Q^2) \frac{dy}{y} \quad (50)$$

In the above expression, μ is the renormalization scale, $\Delta\Sigma(x) = \sum_{i=1}^{n_f} \Delta q_i(x)$ is the singlet (S) quark PPDFs, ΔG is the polarized gluonic distribution function, $\Delta_{NS}(x) = \sum_{i=1}^{n_f} (e_i^2 - \frac{1}{n_f} \sum_{j=1}^{n_f} e_j^2) \Delta q_i(x)$ is the non-singlet (NS) quark PPDFs, $\Delta C_{q,S}^{(n)}$ and $\Delta C_{q,NS}^{(n)}$ are the singlet and non-singlet coefficient functions for the polarized quarks/antiquarks, respectively, and $\Delta C_g^{(n)}$ is the coefficient function for the gluons with $n = 1, 2, 3, \dots$ for $N^{(n)}LO$ [52, 53, 70].

The singlet coefficient function for the quarks is decomposed in terms of non-singlet and pure singlet contributions as

$$\Delta C_{q,S}^{(n)} = \Delta C_{q,NS}^{(n)} + \Delta C_{q,PS}^{(n)}. \quad (51)$$

At NLO, the pure singlet coefficient function $\Delta C_{q,PS}^{(n)} = 0$, and therefore, $\Delta C_{q,S}^{(1)} = \Delta C_{q,NS}^{(1)}$. This leads to [52]:

$$\begin{aligned} g_{1N}(x, Q^2) &= \frac{1}{2} \int_x^1 \frac{dy}{y} \left[\left\{ \frac{1}{n_f} \sum_{j=1}^{n_f} e_j^2 \Delta\Sigma\left(\frac{x}{y}, \mu^2\right) + \Delta_{NS}\left(\frac{x}{y}, \mu^2\right) \right\} \Delta C_{q,NS}^{(1)}\left(y, \frac{Q^2}{\mu^2}\right) \right. \\ &\quad \left. + \frac{1}{n_f} \sum_{j=1}^{n_f} e_j^2 \Delta G\left(\frac{x}{y}, \mu^2\right) \Delta C_g^{(1)}\left(y, \frac{Q^2}{\mu^2}\right) \right] \end{aligned} \quad (52)$$

We have used the following expressions for the quark and gluon coefficient functions at NLO following Refs. [52, 70]:

$$\begin{aligned} \Delta C_{q,NS}^{(1)}(y) &= \frac{\alpha_s(Q^2)}{4\pi} C_F \left[\ln\left(\frac{Q^2}{\mu^2}\right) \left\{ \frac{4}{(1-y)_+} - 2(1+y) + 3\delta(1-y) \right\} + 4 \frac{\ln(1-y)}{(1-y)_+} - \frac{3}{(1-y)_+} \right. \\ &\quad \left. - 2(1+y)\ln(1-y) - 2 \frac{(1+y^2)}{(1-y)} \ln(y) + 4 + 2y + \delta(1-y) \left(-\frac{4\pi^2}{6} - 9 \right) \right], \end{aligned} \quad (53)$$

$$\Delta C_g^{(1)}(y) = \frac{\alpha_s(Q^2)}{4\pi} T_F n_f \left[4(2y-1)\ln\left(\frac{Q^2}{\mu^2}\right) + 4(2y-1)(\ln(1-y) - \ln(y)) + 4(3-4y) \right], \quad (54)$$

with $C_F = 3$, $T_F = \frac{1}{2}$ and $\alpha_s(Q^2)$ as the strong coupling constant. In the limit of $\mu^2 = Q^2$, the above coefficient functions reduce to the coefficient functions given in Ref. [53]. Following the works of Zijlstra et al. [52], we have performed the numerical evaluation of $g_{1N}(x, Q^2)$ up to NNLO.

Following a similar analogy, the unpolarized nucleon structure functions $F_{iN}(x, Q^2)$ ($i = 2, L$) are also expressed in terms of the convolution of parton coefficient function ($C_{i,f}^{(n)}(x)$; ($f = q, g$)) with the parton density distribution ($f(x)$) inside the nucleon as [55, 71–73]:

$$x^{-1} F_{iN}(x) = \sum_{f=q,g} C_{i,f}^{(n)}(x) \otimes f(x), \quad i = 2, L, \quad (55)$$

where $F_{LN}(x)$ is the longitudinal structure function which is zero in the naive quark parton model. However, in the QCD improved parton model because of the quark-quark interaction via gluon, quarks may couple with the longitudinally polarized photons giving rise to nonzero contribution from $F_{LN}(x, Q^2)$ [55]:

$$F_{LN}(x, Q^2) = \left(1 + \frac{4M^2 x^2}{Q^2} \right) F_{2N}(x, Q^2) - 2x F_{1N}(x, Q^2). \quad (56)$$

By using Eq. 56, we have obtained the unpolarized structure function $F_{1N}(x, Q^2)$ beyond the leading order.

For example, the quark coefficient function for $F_{iN}(x, Q^2)$ at NLO is decomposed in terms of singlet and non-singlet contributions as follows [71–73]:

$$C_{i,q}^{(1)}(x) = C_{i,NS}^{(1)}(x) + C_{i,S}^{(1)}(x), \quad (57)$$

After simplification, Eq. 55, is expressed as:

$$\begin{aligned} x^{-1} F_{iN}(x, Q^2) &= \int_x^1 \frac{dy}{y} \left[\frac{1}{n_f} \sum_{j=1}^{n_f} e_j^2 \Sigma\left(\frac{x}{y}, \mu^2\right) C_{i,S}^{(1)}\left(y, \frac{Q^2}{\mu^2}\right) + \Delta_{NS}\left(\frac{x}{y}, \mu^2\right) C_{i,NS}^{(1)}\left(y, \frac{Q^2}{\mu^2}\right) \right. \\ &\quad \left. + \frac{1}{n_f} \sum_{j=1}^{n_f} e_j^2 G\left(\frac{x}{y}, \mu^2\right) C_{i,g}^{(1)}\left(y, \frac{Q^2}{\mu^2}\right) \right] \end{aligned} \quad (58)$$

where $\Sigma(x) \left(= \sum_{i=1}^{n_f} q_i(x) \right)$ and $\Delta_{NS}(x) \left(= \left[\sum_{i=1}^{n_f} e_i^2 - \frac{1}{n_f} \sum_{j=1}^{n_f} e_j^2 \right] q_i(x) \right)$ are the singlet and the non-singlet quark distribution and $G(x)$ is the gluon distribution. $C_{i,NS}(x)$ is the coefficient function for the non-singlet, and $C_{i,q}^{(n)}(x)$ and $C_{i,g}^{(n)}(x)$ are the coefficient functions for the singlet quark and gluon, respectively. It is important to mention that the leading contribution to the coefficient functions for $F_{LN}(x, Q^2)$ is of the first order in the strong coupling constant $\alpha_s(Q^2)$ instead of zeroth order in $\alpha_s(Q^2)$, i.e., $(\alpha_s(Q^2))^0$ as in the case of other structure functions.

More details for the evolution of unpolarized structure functions and nonperturbative QCD corrections have been discussed in an our earlier work [55].

2. Nonperturbative Target Mass Corrections and Twist-3 corrections

After performing the perturbative evolution of parton densities up to NNLO, we have incorporated the nonperturbative target mass correction effect as well as the twist-3 effects which are related with the quark-gluon correlations in a nucleon following Refs. [45, 54, 74].

The target mass corrected polarized structure function is now given by [45, 74]:

$$\begin{aligned} g_{1N}^{TMC}(x, Q^2) &= \frac{1}{(1+\gamma^2)^{3/2}} \frac{x}{\xi} g_{1N}(\xi, Q^2) + \frac{\gamma^2}{(1+\gamma^2)^2} \int_{\xi}^1 \frac{dv}{v} \left\{ \frac{x+\xi}{\xi} \right. \\ &\quad \left. + \frac{\gamma^2-2}{2\sqrt{1+\gamma^2}} \log\left(\frac{v}{\xi}\right) \right\} g_{1N}(v, Q^2), \end{aligned} \quad (59)$$

where $\xi = \frac{2x}{1+\sqrt{1+\gamma^2}}$ and $\gamma^2 = \frac{4M^2x^2}{Q^2}$.

The twist-3 corrected structure function is given by [54]:

$$\begin{aligned} g_{1N}^{\tau=3}(x, Q^2) &= \frac{\gamma^2}{(1+\gamma^2)^{3/2}} g_{1N}(\xi, Q^2) - \frac{3\gamma^2}{(1+\gamma^2)^2} \int_{\xi}^1 \frac{dv}{v} g_{1N}(v, Q^2) \\ &\quad + \frac{\gamma^2(2-\gamma^2)}{(1+\gamma^2)^{5/2}} \int_{\xi}^1 \frac{dv}{v} \log\left(\frac{v}{\xi}\right) g_{1N}(v, Q^2) \end{aligned} \quad (60)$$

Hence, with the perturbative and nonperturbative QCD corrections, the polarized structure function $g_{1N}(x, Q^2)$ is given by

$$g_{1N}(x, Q^2) = \underbrace{g_{1N}^{(n)}(x, Q^2)}_{pQCD(n=0,1,2,\dots)} + g_{1N}^{TMC}(x, Q^2) + \underbrace{g_{1N}^{\tau=3}(x, Q^2)}_{higher\ twist} \quad (61)$$

leading twist ($\tau=2$)

In an our earlier work [55], we have already discussed the effects of target mass and higher twist corrections for the unpolarized nucleon structure functions $F_{1N}(x, Q^2)$ and $F_{2N}(x, Q^2)$ in detail. Following our earlier works. [55], the

expressions for the target mass corrected structure functions are given by:

$$F_{2N}^{TMC}(x, Q^2) \approx \frac{x^2}{\xi^2 \gamma'^3} F_{2N}(\xi) (1 + 6r(1 - \xi)^2), \quad (62)$$

$$F_{1N}^{TMC}(x, Q^2) \approx \frac{x}{\xi r} F_{1N}(\xi) (1 + 2r(1 - \xi)^2), \quad (63)$$

In the above expressions, $\xi = \frac{2x}{1 + \sqrt{1 + \frac{4M^2 x^2}{Q^2}}}$, $r = \frac{\mu x \xi}{\gamma'}$, $\mu = \left(\frac{M}{Q}\right)^2$ and $\gamma' = \sqrt{1 + \frac{4M^2 x^2}{Q^2}}$, respectively.

IV. RESULTS AND DISCUSSION

We have obtained the numerical results for the unpolarized structure functions $F_{1,2}^{p,n}(x, Q^2)$ using Eqs. 8 and 15 of Ref. [55], polarized structure functions $g_{1p,2p}(x, Q^2)$, $g_{1n,2n}(x, Q^2)$ using Eqs. 50 and 61, and nucleon asymmetries $A_{1p,2p}(x, Q^2)$ using Eqs. 26 and 27. We have also studied the sum rules for the polarized structure functions $g_{1p,1n}(x, Q^2)$ and $g_{2p}(x, Q^2)$ given by Ellis-Jaffe [65], Bjorken [30], and Burkhardt-Cottingham [66] as well as the Gottfried sum rule [59] for the unpolarized structure function $F_{2p,2n}(x, Q^2)$ in section IV E.

All the numerical results are obtained for the kinematic region of $Q^2 \geq 1 \text{ GeV}^2$ with the target mass correction effect. We have also included the twist-3 correction (wherever mentioned) in our numerical calculations. These results are presented and discussed below. The present results have been compared with some of the experimental results [1, 4–23, 75–83] from EMC, E142, E143, E154, E155, HERMES, SMC, CLAS, NMC, BCDMS, SLAC and COMPASS. Some of the experimental results have been obtained with a kinematic cut of 2 GeV on the center of mass energy W , defined as

$$W = \sqrt{M^2 + Q^2 \left(\frac{1}{x} - 1\right)} \quad (64)$$

and therefore, we have obtained the numerical results without and with a cut of $W \geq 2 \text{ GeV}$.

A. Polarized proton and neutron structure functions $g_1^{p,n}(x, Q^2)$

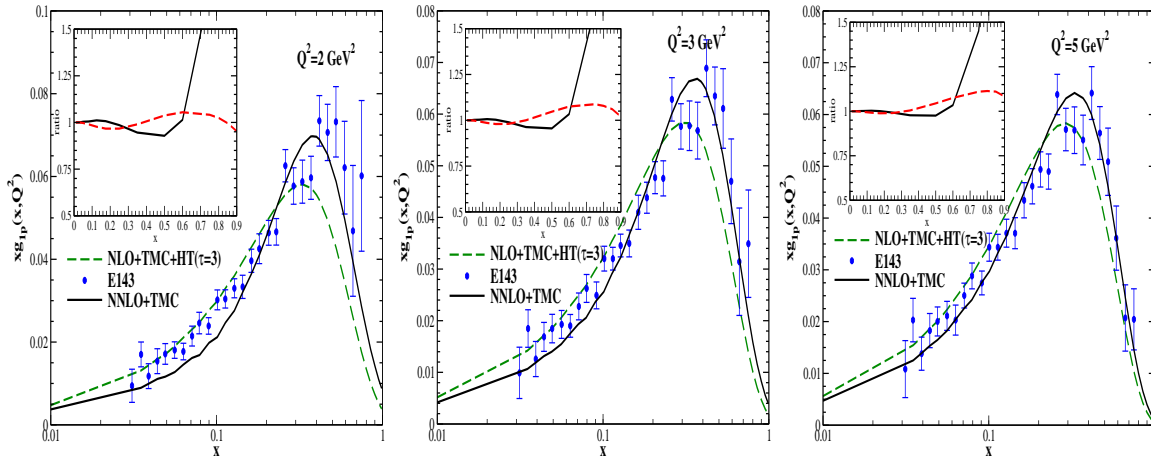


FIG. 1: $xg_{1p}(x, Q^2)$ vs x at the different values of Q^2 at (i) NLO with TMC and twist-3 correction (dashed line) and (ii) NNLO incorporating the TMC effect (solid line), without applying any constraint on the center of mass energy W . Numerical results are compared with the E143 experimental data [5]. In the inset of these figures the ratios of the numerical results (i) with the TMC and twist-3 corrections to the results with TMC effect only at NLO (dashed line) and (ii) with the TMC to the results without TMC effect at NLO (solid line) have been shown.

In Fig. 1, we have shown the results for $xg_{1p}(x, Q^2)$ vs x , obtained at the different values of Q^2 viz. 2, 3 and 5 GeV^2 . The numerical results are obtained at NLO with twist-3 correction (dashed lines) and at NNLO (solid lines).

In the inset of the figure, we present the ratios $\frac{g_{1p}^{(NLO+TMC)}(x, Q^2)}{g_{1p}^{(NLO)}(x, Q^2)}$ (solid lines) and $\frac{g_{1p}^{p(NLO+TMC+\tau=3)}(x, Q^2)}{g_{1p}^{(NLO+TMC)}(x, Q^2)}$ (dashed lines) showing the effect of nonperturbative target mass and twist-3 corrections, respectively. It may be noticed that TMC effect is more pronounced as compared to the twist-3 correction and rises sharply for $x > 0.6$. We find that twist-3 corrections are small (< 1%) in the present kinematic region which decreases with the increase in Q^2 . Therefore, we have not included twist-3 contribution in the results obtained for the various cases hereafter in Figs. 2-13. Moreover, in Fig. 1 the results evaluated at NLO are higher than the results evaluated at NNLO in the region of low x while it seems smaller for high x region. For example, up to $x < 0.2$ the numerical results at NNLO are lower than the results obtained at NLO, however, at $x \simeq 0.2$ there is a cross over and for $x > 0.2$ the results at NNLO become higher than the results at NLO. Quantitatively, at $x = 0.1$ this difference is found out to be 30%, which becomes 8% at $x = 0.3$, 46% at $x = 0.5$ and 70% at $x = 0.75$ for $Q^2 = 2 \text{ GeV}^2$. We find that this difference decreases with the increase in Q^2 and it becomes 28% at $x = 0.1$, 7% at $x = 0.3$, 32% at $x = 0.5$ and 56% at $x = 0.75$ for $Q^2 = 5 \text{ GeV}^2$. Furthermore, we have compared the numerical results with the experimental data of E143 [5]. From the figure, it may be noticed that our results for $xg_{1p}(x, Q^2)$ show qualitatively good agreement with the experimental data at all the values of Q^2 considered here. At higher values of Q^2 the numerical results at NNLO are in better agreement with the experimental data.

In Fig. 2, we have shown the results for $g_{1p}(x, Q^2)$ vs x at the different values of Q^2 . The numerical results are obtained by performing the PPDFs evolution up to NNLO in the region of $1 \leq Q^2 \leq 5 \text{ GeV}^2$ (left panel: shown by a shaded band), at $Q^2 = 10 \text{ GeV}^2$ (middle panel) and for a wide range of Q^2 ($1 \leq Q^2 \leq 58 \text{ GeV}^2$: right panel) with a kinematical cut of $W \geq 2 \text{ GeV}$. We find that $g_{1p}(x, Q^2)$ decreases with the increase in x while it increases with the increase in Q^2 . One may notice that at all values of Q^2 considered here, NLO results are higher than the results evaluated at NNLO for low x region and show opposite trend for high x region. The difference in the results due to the higher order corrections is observed to be more pronounced in the region of low x and low Q^2 and decreases with the increase in x and Q^2 (though remain significant). The obtained results are compared with the experimental data of CLAS [21] and SMC [10]. It may be noticed from the figure that our numerical results show good agreement with the experimental data in the entire range of Bjorken x .

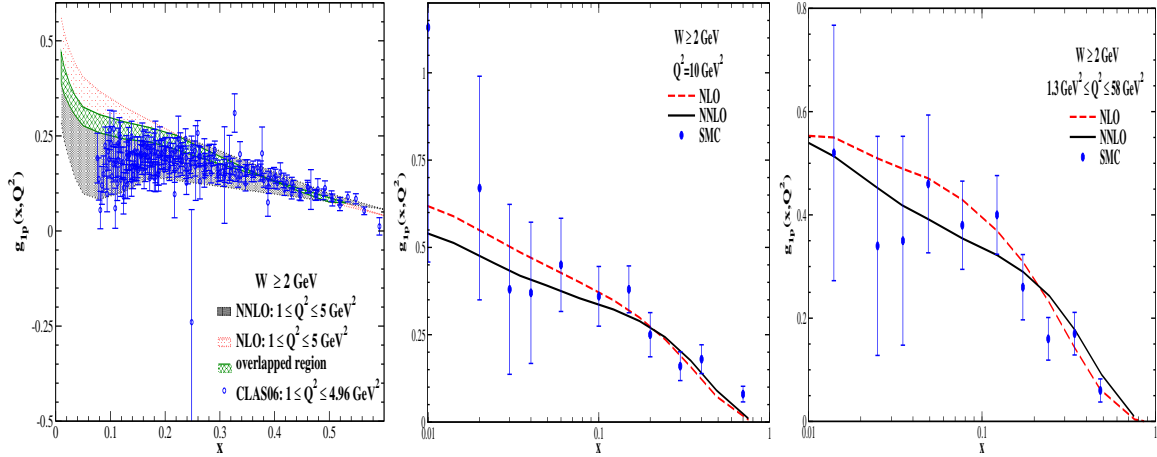


FIG. 2: $g_{1p}(x, Q^2)$ vs x **Left panel:** at NLO (a band with dotted pattern) and at NNLO (a band with shaded pattern) with the TMC effect for $1 \leq Q^2 \leq 5 \text{ GeV}^2$ and the overlapped region of these results is shown by a band with cross pattern, **Middle panel:** at NLO (dashed line) and NNLO (solid line) with the TMC effect at $Q^2 = 10 \text{ GeV}^2$ **Right panel:** at NLO (dashed line) and NNLO (solid line) with TMC effect for $1.3 \leq Q^2 \leq 58 \text{ GeV}^2$ corresponding to the experimental data from SMC [10]. These numerical results are obtained by applying a kinematic constraint of 2 GeV on the center of mass energy W and are compared with SMC [10] (solid circles) and CLAS06 [21] (open circles) experimental data.

To observe the Q^2 -dependence of the polarized structure function $g_{1p}(x, Q^2)$, in Fig. 3, we have shown the numerical results for $g_{1p}(x, Q^2)$ vs Q^2 at fixed values of x in the kinematic region of $0.0063 \leq x < 0.8$ and $1 \leq Q^2 \leq 60 \text{ GeV}^2$ without applying any cut on the center of mass energy W . The numerical results are obtained at NLO (dashed lines) and NNLO (solid lines) with the target mass correction effect. One may notice from the figure that for a given value of x , the proton structure function gets almost saturated in the region of high Q^2 . Here also, we observe a difference in the results due to the higher order perturbative evolution of parton densities at NLO and NNLO that is more pronounced at lower values of x and becomes small with the increase in x and Q^2 . For example, at $x = 0.049$ this difference is found to be 24% at $Q^2 = 2 \text{ GeV}^2$, 18% at $Q^2 = 5 \text{ GeV}^2$ and 12% at $Q^2 = 10 \text{ GeV}^2$. However, at $x = 0.346$, it becomes 16%, 14% and 10% at $Q^2 = 2, 5, 10 \text{ GeV}^2$, respectively. Furthermore, we have compared

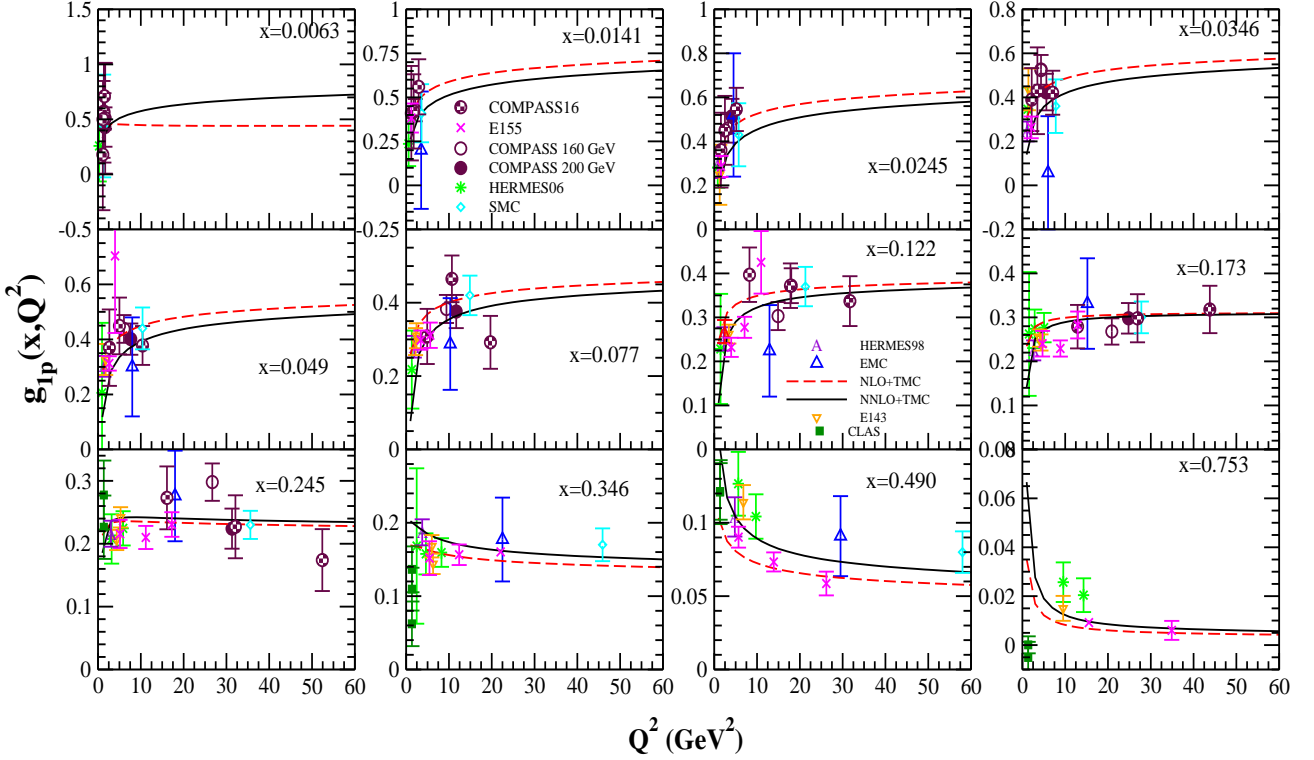


FIG. 3: $g_{1p}(x, Q^2)$ vs Q^2 at the different values of x . These results are shown at NLO and NNLO incorporating the TMC effect for $1 \leq Q^2 \leq 60$ GeV^2 and are compared with the available experimental data from EMC [1] (triangle up symbol), E143 [5] (triangle down symbol), E155 [8] (cross symbol), SMC [10] (open diamond symbol), COMPASS [13, 14] (circle symbols), HERMES [16, 17] (star and character symbols) and CLAS [19] (solid square symbol) experiments.

the numerical results with the data available from the EMC [1], E143 [5], E155 [8], SMC [10], COMPASS [13, 14], HERMES [16, 17] and CLAS [19] experiments. From the figure, it may be noticed that our results at NNLO show good agreement with the experimental data for the entire range of x considered in this work.

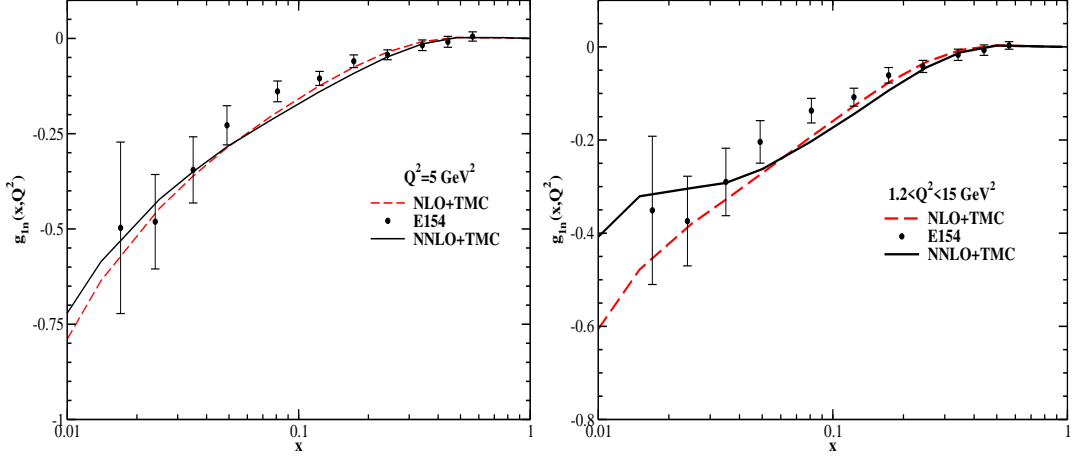


FIG. 4: $g_{1n}(x, Q^2)$ vs x at NLO and NNLO with the TMC effect at $Q^2 = 5$ GeV^2 (left panel) and for $1.2 \leq Q^2 \leq 15$ GeV^2 (right panel) corresponding to the experimental data from E154 [6].

In Fig. 4, the numerical results are presented for the polarized neutron structure function $g_{1n}(x, Q^2)$ vs x at NLO as well as at NNLO. In the left panel, the results are shown for a fixed value of Q^2 viz. $Q^2 = 5$ GeV^2 , while in the right panel, Q^2 has been varied in the range $1.2 \leq Q^2 \leq 15$ GeV^2 corresponding to the experimental data of E154 [6]. These results are obtained without applying any cut on W . One may notice that for a neutron target the

polarized structure function has a negative sign due to the dominance of down quarks and approach to zero with the increases in x while the proton structure function $g_{1p}(x, Q^2)$ has a positive sign and decreases with the increase in x . Additionally, we find that perturbative higher order corrections of the polarized parton densities exhibit qualitatively similar behavior to what we have seen in the case of proton target. From the figure, it may be observed that our results at NNLO show a very good agreement with the E154 experimental data [6]. It is important to point out that the experimental data have larger uncertainties in the region of low $x < 0.1$, where the helicity distributions of quarks and gluons are not well established.

B. Polarized proton and neutron structure functions $g_{2p,2n}(x, Q^2)$

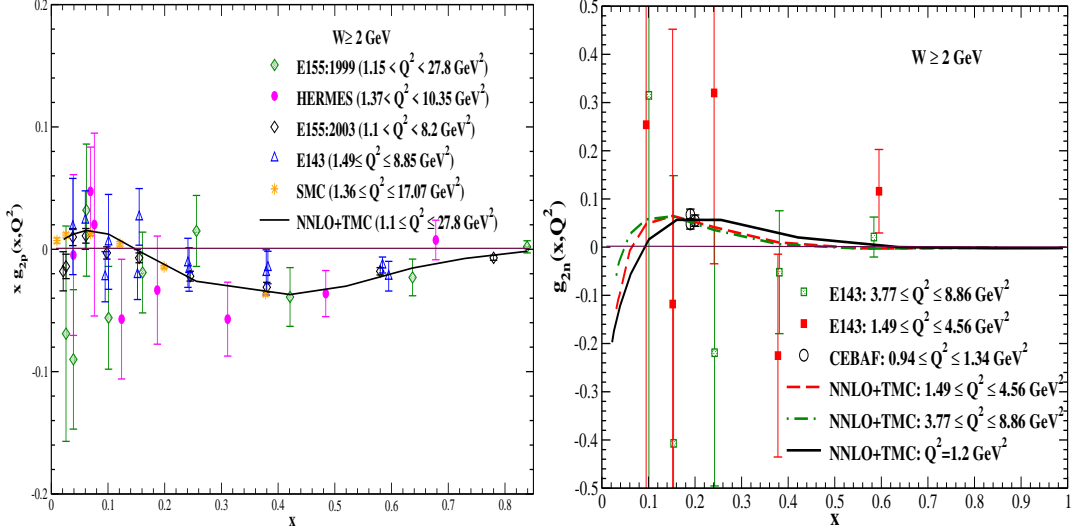


FIG. 5: $x g_{2p}(x, Q^2)$ (left panel) and $g_{2n}(x, Q^2)$ (right panel) vs x at NNLO with TMC effect in the kinematic region of $W \geq 2$ GeV and Q^2 as mentioned in the legends of the figures. The numerical results are compared with the experimental data of E143 [5], E155 [7, 9], SMC [11], HERMES [18] and CEBAF [20] experiments.

In Fig. 5 (left panel), we have shown the results for $x g_{2p}(x, Q^2)$ vs x in the range of $1.1 \leq Q^2 \leq 27.8 \text{ GeV}^2$ corresponding to the kinematic regions of the various experiments, i.e., E143 [5], E155 [7, 9], SMC [11] and HERMES [18], and in the right panel of this figure, the numerical results are presented for $g_{2n}(x, Q^2)$ vs x at the different values of Q^2 corresponding to the available experimental data from E143 [5] and CEBAF [20] collaborations. These numerical results are evaluated at NNLO incorporating the target mass correction effect using the Wandzura-Wilczek relation given in Eq. 50. Furthermore, a kinematic cut of 2 GeV has also been applied on the center of mass energy W . We find that in the present kinematic region, there is very small difference between the results evaluated at NLO and NNLO, therefore, we show the results in the case of NNLO only. One may observe that corrections to the QPM are non-negligible in the region of intermediate x which results a difference of $\simeq 3\%$ at $x = 0.25$, 4% at $x = 0.4$ and about 2% at $x = 0.65$ in the numerical results of $x g_{2p}(x, Q^2)$ from the QPM value which is zero. However, this difference decreases with the increase in x and Q^2 . In the right panel, the numerical results for $g_{2n}(x, Q^2)$ are shown and we find that at $Q^2 = 1.2 \text{ GeV}^2$ due to the higher order QCD corrections to QPM there is a difference of about 20% at $x = 0.02$ which decreases to 12% at $x = 0.04$, about 2% at $x = 0.1$ and 6% at $x = 0.25$. It may be noticed that $g_{2n}(x, Q^2)$ becomes almost negligible for $x > 0.4$ irrespective of the values of Q^2 taken into consideration. The available experimental data have large error bars except those reported from the E155 [9] and SMC [11] collaborations, which are in very good agreement with our numerical results for the polarized proton target. It may also be noticed from the figure that our results for $x g_{2p}(x, Q^2)$ have been found out to be in reasonable agreement with the experimental data reported from the experiments performed at SLAC, CERN and DESY collaborations [5, 7, 9, 11, 18] in the entire range of Bjorken x . The numerical results for $g_{2n}(x, Q^2)$ are also in agreement with the experimental results reported from CEBAF [20]. It may be noticed that the experimental data from E143 [5] have large error bars due to the large systematic and statistical uncertainties in the measurements.

C. Unpolarized proton structure functions $F_{1,2}^p(x, Q^2)$

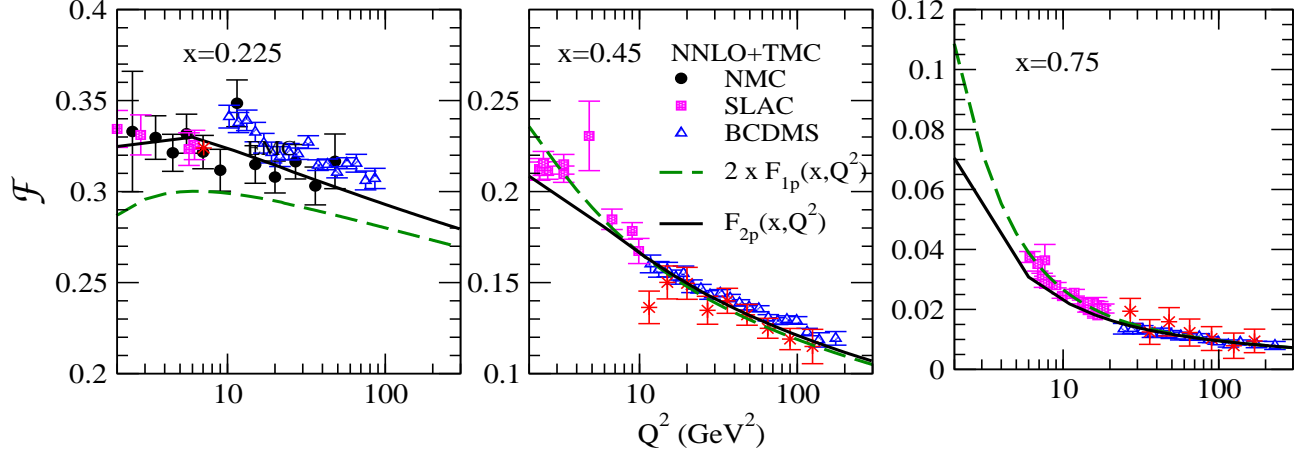


FIG. 6: $\mathcal{F} = F_{2p}(x, Q^2)$ (solid lines) and $\mathcal{F} = 2x F_{1p}(x, Q^2)$ (dashed lines) vs Q^2 are shown at different x for the case of free proton [55]. The results are obtained at NNLO including the target mass correction effect and are compared with the available experimental data from BCDMS [80], SLAC [81], NMC [82] and EMC [83] experiments.

In Fig. 6, the numerical results are presented for the structure functions $F_{2p}(x, Q^2)$ and $2x F_{1p}(x, Q^2)$ vs Q^2 at NNLO for the unpolarized proton target, and the evolution of unpolarized parton densities is performed using the PDF parameterization of Martin, Motylinski, Harland-Lang, Thorne (MMHT) 2014 for the nucleons [84]. These results are obtained at the different values of x for a wide range of Q^2 . We find that in the region of low x , there is significant difference between the results of $F_{2p}(x, Q^2)$ and $2x F_{1p}(x, Q^2)$ which shows that Callan-Gross (CG) relation gets violated due to the inclusion of higher order perturbative as well as nonperturbative QCD corrections. It may be noticed from the figure that in the region of intermediate and high x this difference becomes negligible for $Q^2 > 10$ GeV^2 while it is still significant for $Q^2 \lesssim 10$ GeV^2 . We have also compared the results of $F_{2p}(x, Q^2)$ with the available experimental data from BCDMS [80], SLAC [81], NMC [82] and EMC [83] experiments, and find a reasonably good agreement between the theoretical and experimental results. These results are taken from our earlier work [55]. We have used these numerical results in the evaluation of the spin asymmetries $A_{1p}(x, Q^2)$ and $A_{2p}(x, Q^2)$ discussed in the following subsection.

D. Spin asymmetries

In Fig. 7, the numerical results are presented for the spin asymmetries $A_{1p}(x, Q^2)$ (left panel) and $A_{2p}(x, Q^2)$ (right panel) using Eqs. 26 and 27 at NNLO including the TMC effect. These results are presented in the kinematic region of $W \geq 2$ GeV . It may be noticed that the asymmetry $A_{1p}(x, Q^2)$ is small in the region of low x , however, it increases with the increase in x and approaches unity for $x \rightarrow 1$. It implies that in the region of high x , quarks are carrying most of the momentum fraction of the target nucleon as well as most of its spin fraction. We find that higher order QCD corrections to the leading order results of $A_{1p}(x, Q^2)$ (not shown here explicitly) are significant in the entire range of x and leads to a difference of 18% at $x = 0.05$, 12% at $x = 0.128$, 4% at $x = 0.3$ and 10% for your reference at $x = 0.74$ for the Q^2 range of E143 experiment [5]. We have also compared our numerical results with the experimental data from E143 [5], SMC [10] and COMPASS16 [14] and find them in fair agreement in the entire range of x . In the right panel, we show the numerical results for $A_{2p}(x, Q^2)$ and its comparison with experimental data from E143 [5] and E155 [9]. It may be noticed that $A_{2p}(x, Q^2)$ is small in magnitude than $A_{1p}(x, Q^2)$, as it is suppressed by a factor of $\gamma = \sqrt{\frac{4M^2x^2}{Q^2}}$ (see Eq. 27). Consequently, we find that at low $x (< 0.1)$, $A_{2p}(x, Q^2)$ is very small, it increases with the increase in x and then saturates. On comparing the theoretical curves for the different ranges of Q^2 , we observe that A_{2p} decreases with the increase in Q^2 . The numerical results have been compared with the corresponding experimental data from E143 [5] and E155 [9] and are found to be in reasonable agreement with them. These results for $A_{2p}(x, Q^2)$ are important to get information about the transverse polarization of quark spins.

In Fig. 8, we have presented the results for the ratio of polarized to unpolarized proton (left panel) and neutron

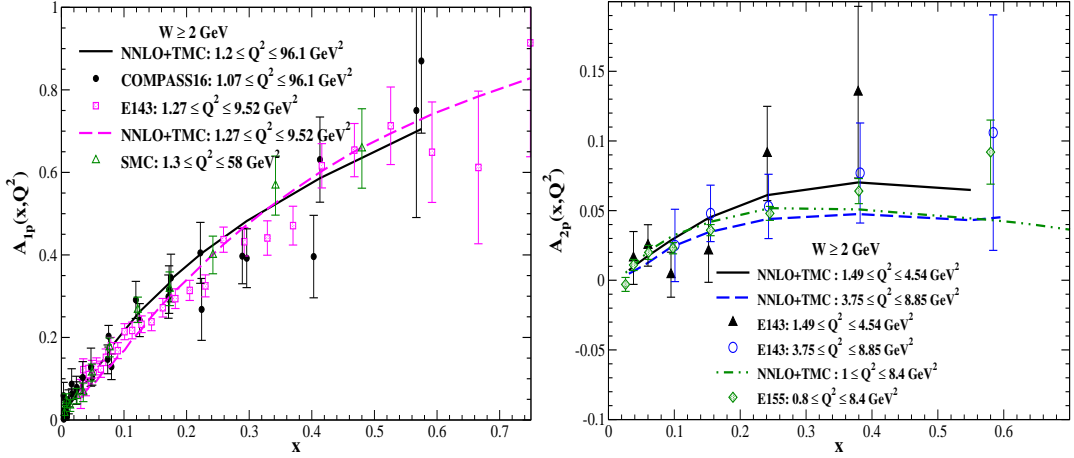


FIG. 7: The results for $A_{1p}(x, Q^2)$ (left panel) and $A_{2p}(x, Q^2)$ (right panel) vs x are shown. These results are obtained at NNLO with the TMC effect in the different ranges of Q^2 corresponding to the available data from E143 [5], E155 [9], SMC [10] and COMPASS16 [14] experiments as mentioned in the legends of the figure.

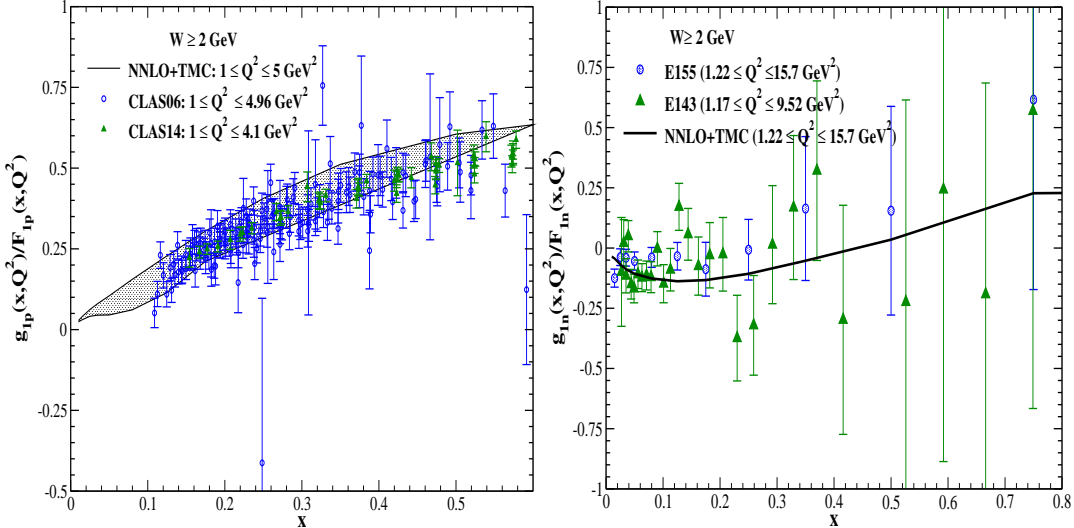


FIG. 8: **Left panel:** Results for the ratio $g_{1p}(x, Q^2)/F_{1p}(x, Q^2)$ at NNLO incorporating the TMC effect for $1.0 \leq Q^2 \leq 5.0 \text{ GeV}^2$ and are compared with the results of CLAS06 [21] and CLAS14 [22] experimental data. **Right panel:** Results for the ratio $g_{1n}(x, Q^2)/F_{1n}(x, Q^2)$ vs x at NNLO with the TMC effect for $1.2 \leq Q^2 \leq 15.7 \text{ GeV}^2$ corresponding to the experimental data of E143 [5] and E155 [8].

(right panel) structure functions, i.e., $\frac{g_{1p}(x, Q^2)}{F_{1p}(x, Q^2)}$ and $\frac{g_{1n}(x, Q^2)}{F_{1n}(x, Q^2)}$ evaluated at NNLO. These results are obtained in the different ranges of Q^2 corresponding to the kinematic range of E143 [5], E155 [8] and CLAS [21, 22] experiments. The numerical results of $\frac{g_{1p}(x, Q^2)}{F_{1p}(x, Q^2)}$ show similar qualitative behavior as we have observed in the case of spin asymmetries $A_{1p}(x, Q^2)$. We find that the higher order perturbative corrections to the QPM are important in the evaluation of ratio $\frac{g_{1p}(x, Q^2)}{F_{1p}(x, Q^2)}$ and due to their inclusion a difference of about 56% is found at $x = 0.05$ which reduces to 30% at $x = 0.175$ for $Q^2 = 1 \text{ GeV}^2$. However, with the increase in Q^2 these corrections to QPM become small, for example, at $Q^2 = 5 \text{ GeV}^2$ the difference in the ratio evaluated at LO and NNLO becomes 4% at $x = 0.05$, 8% at $x = 0.125$, 15% at $x = 0.5$ and 17% at $x = 0.6$. It may be noticed that our numerical results shown by the band covering the kinematic region of $1.0 \leq Q^2 \leq 5.0 \text{ GeV}^2$ and $W \geq 2 \text{ GeV}$, are in qualitatively good agreement with the experimental data reported from CLAS [21, 22]. In the right panel, the numerical results for $\frac{g_{1n}(x, Q^2)}{F_{1n}(x, Q^2)}$ are shown at NNLO and compared with the experimental results in the kinematic region of $1.2 \leq Q^2 \leq 15.7 \text{ GeV}^2$. This ratio of neutron increases with the increase in x . The perturbative corrections to the QPM results are also found to be significant for

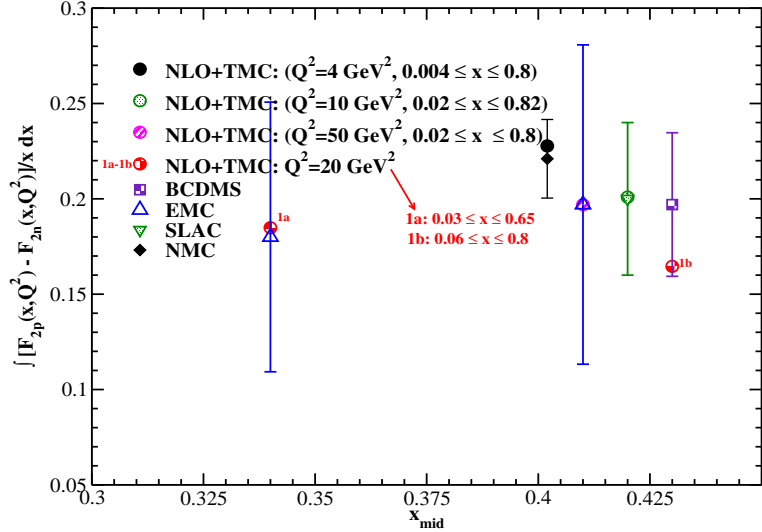


FIG. 9: $S_G = \int_{x_{min}}^{x_{max}} F_{2p}(x, Q^2) dx - \int_{x_{min}}^{x_{max}} F_{2n}(x, Q^2) dx$ vs $x_{mid} \left(= \frac{x_{min} + x_{max}}{2} \right)$ at NLO with TMC effect at the different values of Q^2 . Numerical results are shown by the circle symbol identified by a number and compared with SLAC [75], EMC [76, 77], BCDMS [78] and NMC [79].

$\frac{g_{1n}(x, Q^2)}{F_{1n}(x, Q^2)}$, quantitatively their inclusion cause a difference of about 13% at $x = 0.125$, 42% at $x = 0.35$ and 88% at $x = 0.75$. However, $\frac{g_{1n}(x, Q^2)}{F_{1n}(x, Q^2)}$ show similar qualitative dependence on x and Q^2 as we have observed in the case of proton target. The experimental data of E143 [5] and E155 [8] have larger uncertainties in the region of intermediate and high $x (> 0.4)$. Our numerical results are found to be consistent when compared with the experimental data in the entire range of x considered here.

E. Various sum rules

We have applied our formalism given in Ref. [55] to evaluate the Gottfried sum rule for the unpolarized proton and neutron structure functions ($F_{2p}(x, Q^2)$ and $F_{2n}(x, Q^2)$) for which the results are presented in Fig. 9. The numerical results are obtained at NLO with the TMC effect in the kinematic region of $0.004 \leq x \leq 0.82$ and at Q^2 corresponding to the experimental data. We find that the numerical results are suppressed as compared to the predicted value of $1/3$ (Eq. 28) for the flavor symmetric sea which implies that $\bar{u} \neq \bar{d}$ and the abundance of one flavor over other is responsible for the missing contribution. It may be observed from the figure that our numerical results are in good agreement with the experimental findings of SLAC [75], EMC [76, 77], BCDMS [78] and NMC [79].

In Figs. 10, 11 and 12, the results are presented for the integral of the proton and neutron polarized structure functions $g_{1p}(x, Q^2)$ and $g_{1n}(x, Q^2)$ in the different limits of integration at NNLO. The obtained numerical results are shown by the circle symbol (which has been assigned a number to correspond to the kinematical constrain applied by the respective experiment) and compared with the experimental results from the E142 [4], E155 [8], SMC [11, 12], HERMES [17], etc. available in the literature. We find that perturbative higher order corrections are significant in the entire range of $x (0 \leq x \leq 1)$, and become small with the increase in Q^2 . For example, in the results of S_{EJ}^p evaluated at NNLO (shown in Fig. 10) there is a difference of about 10% from the QPM results at $Q^2 = 1 \text{ GeV}^2$ which reduces to 5% at $Q^2 = 2 \text{ GeV}^2$ and 2% at $Q^2 = 5 \text{ GeV}^2$. This difference is found to be more pronounced for S_{EJ}^n (shown in Fig. 11), quantitatively it is about 10%-14% for $1 \leq Q^2 \leq 5 \text{ GeV}^2$. It may be noticed that our results are in very good agreement within the uncertainty of experimental data for the polarized proton target, however, for the polarized neutron target, more theoretical as well as experimental efforts are needed as the error bars are large. This is particularly the case at low Q^2 , while with the increase in Q^2 the difference between our results and the experimental data becomes comparatively small. From the figure, one may notice that the experimental data have large error bars. Hence, improved experimental measurements with higher statistics are required.

In Fig. 12, the numerical results for the Bjorken sum rule are presented and these results also observed to have significant difference at NNLO from the QPM results which is about 12% at $Q^2 = 1 \text{ GeV}^2$, 7% at $Q^2 = 2 \text{ GeV}^2$ and 5% at $Q^2 = 5 \text{ GeV}^2$ in the integration limits of x ranging from 0 to 1. Furthermore, it may also be observed that these numerical results at NNLO show qualitatively good agreement with the corresponding experimental data of

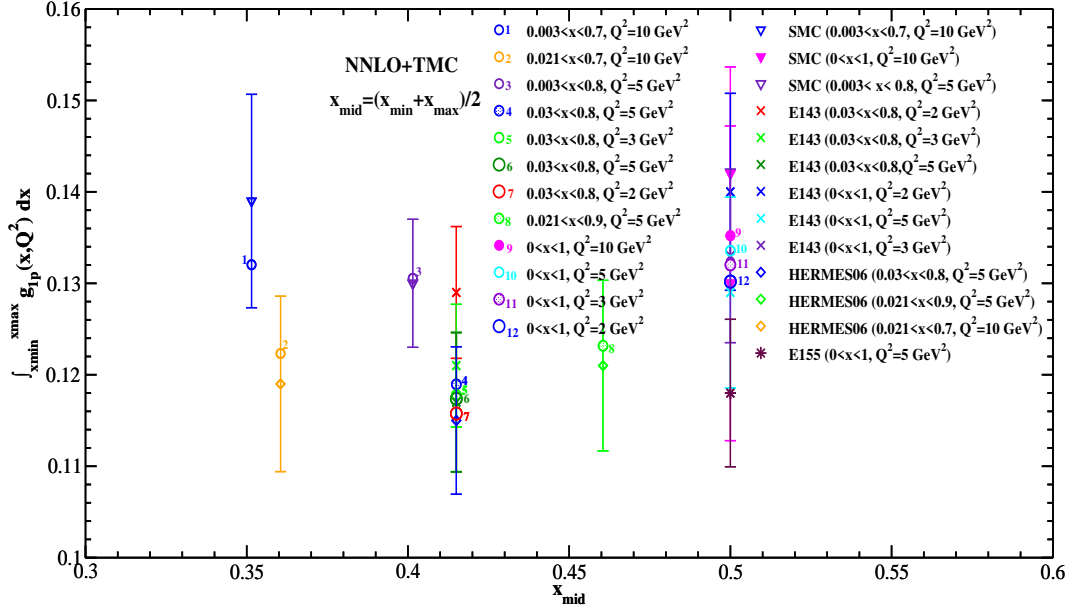


FIG. 10: $S_{EJ}^p = \int_{x_{min}}^{x_{max}} g_{1p}(x, Q^2) dx$ vs x_{mid} ($= \frac{x_{min}+x_{max}}{2}$) at NNLO with the TMC effect for the different values of Q^2 . Our results have been shown by circle symbol identified by a number. The numerical results are obtained in the integration limits of $0 \leq x \leq 1$ at $Q^2 = 2, 3, 5$ and 10 GeV^2 , $0.021 \leq x \leq 0.7$ at $Q^2 = 10 \text{ GeV}^2$, $0.021 \leq x \leq 0.9$ at $Q^2 = 5 \text{ GeV}^2$, $0.003 \leq x \leq 0.8$ at $Q^2 = 5 \text{ GeV}^2$, $0.003 \leq x \leq 0.7$ at $Q^2 = 10 \text{ GeV}^2$ and $0.03 \leq x \leq 0.8$ at $Q^2 = 2, 3$ and 5 GeV^2 corresponding to the experimental data from E143 [5] (cross symbol), E155 [8] (star symbol), SMC [10] (triangle down symbol) and HERMES06 [17] (diamond symbol) experiments.

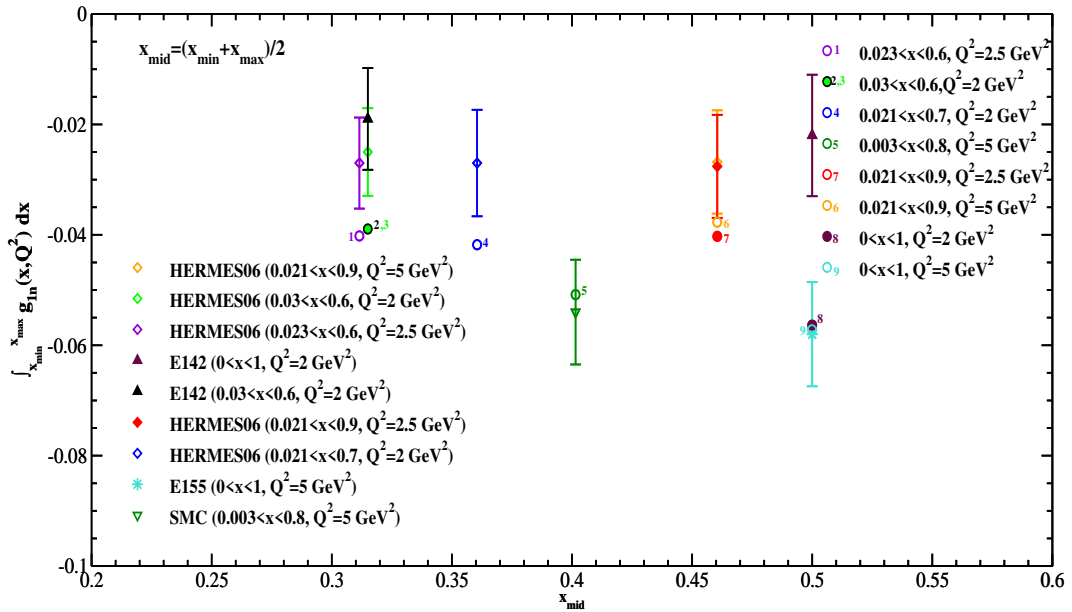


FIG. 11: $S_{EJ}^n = \int_{x_{min}}^{x_{max}} g_{1n}(x, Q^2) dx$ vs x_{mid} ($= \frac{x_{min}+x_{max}}{2}$) at NNLO with the TMC effect for the different values of Q^2 . Our results have been shown by the circle symbol identified by a number. The numerical results are obtained in the integration limits of $0.03 \leq x \leq 0.6$ and $0.021 \leq x \leq 0.7$ at $Q^2 = 2 \text{ GeV}^2$, $0.023 \leq x \leq 0.6$ at $Q^2 = 2.5 \text{ GeV}^2$ and $0.021 \leq x \leq 0.9$ at $Q^2 = 2.5 \text{ GeV}^2$ as well as at $Q^2 = 5 \text{ GeV}^2$ corresponding to the experimental data from E142 [4] (triangle up symbol), E155 [8] (star symbol), SMC [12] (triangle down symbol) and HERMES06 [17] (diamond symbol) experiments.

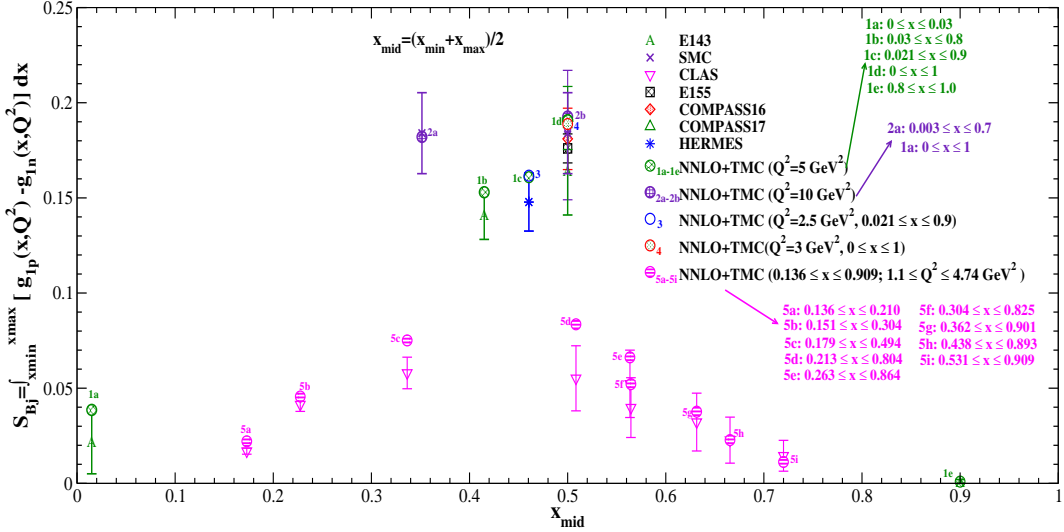


FIG. 12: $S_{Bj} = \int_{x_{min}}^{x_{max}} g_{1p}(x, Q^2) dx - \int_{x_{min}}^{x_{max}} g_{1n}(x, Q^2) dx$ vs $x_{mid} \left(= \frac{x_{min} + x_{max}}{2} \right)$ at NNLO with TMC effect at the different values of Q^2 . Numerical results are shown by the circle symbol identified by a number. The integration limits (as mentioned in the legends of the figure) are chosen corresponding to the experimental data available in the literature. Numerical results are compared with the data reported from E143 [5], E155 [8], SMC [11, 12], COMPASS16 [14], COMPASS17 [15], HERMES [17] and CLAS [23] experiments.

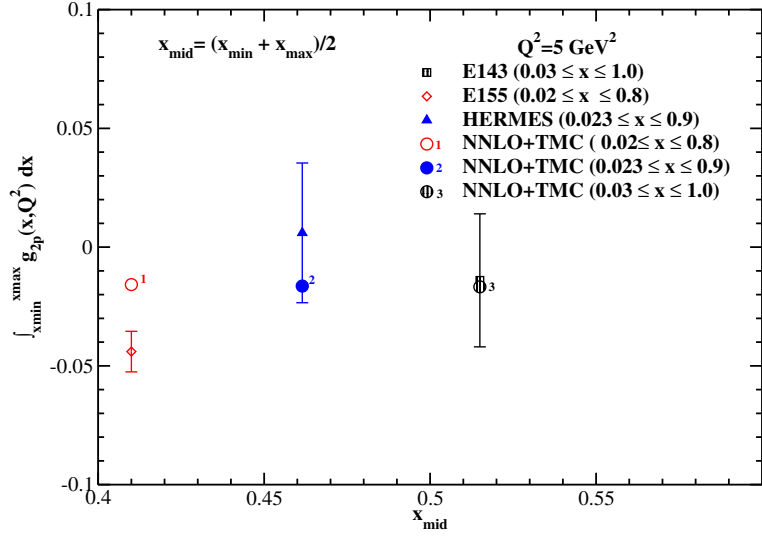


FIG. 13: $\int_{x_{min}}^{x_{max}} g_{2p}(x, Q^2) dx$ vs $x_{mid} \left(= \frac{x_{min} + x_{max}}{2} \right)$ at NNLO with TMC effect at $Q^2 = 5 \text{ GeV}^2$. Numerical results are shown by the circle symbol identified by a number and compared with E143 [5], E155 [9] and HERMES [18] experimental data.

E143 [5], E155 [8], SMC [11, 12], COMPASS16 [14], COMPASS17 [15], HERMES [17] and CLAS [23]. Quantitatively, the numerical value of S_{Bj} is 0.19 in the integration range of $0 \leq x \leq 1$, and it is consistent with the value of Bjorken sum rule, i.e., 0.182 ± 0.002 at the average value of $Q^2 = 5 \text{ GeV}^2$ of the experimental data shown here [85]. These results are in agreement within a difference of 4%, hence may be useful to test the Q^2 evolution as well as the value of strong coupling constant.

In Fig. 13, the results are presented for the Burkhardt-Cottingham sum rule at a fixed $Q^2 = 5 \text{ GeV}^2$. Our numerical results for the polarized proton target are found to be consistent with Eq. 50 as well as with the experimental data from E143 and HERMES. Although there is a difference between the experimental findings of E155 and our theoretical predictions. Since our calculations for $g_{2p}(x, Q^2)$ are limited up to twist-2 contribution so there may be some improvement when the higher twist corrections will be incorporated. In the literature, some authors [41, 44, 54] have discussed about the extraction of higher twist correction using the measurements of $g_2(x, Q^2)$ along with the

world experimental data for $g_1(x, Q^2)$, but a satisfactory theoretical model describing this correction is still lacking.

V. SUMMARY AND CONCLUSION

To conclude, we have studied the effects of perturbative and nonperturbative QCD corrections to the QPM in the evaluation of polarized and unpolarized nucleon structure functions. The numerical calculations are performed up to NNLO using LSS05 PDFs in the 3-flavor MSbar scheme. Moreover, the nonperturbative effects of target mass correction and the twist-3 correction are also incorporated. The results are presented for the polarized proton and neutron structure functions, $g_{1p,1n}(x, Q^2)$ and $g_{2p,2n}(x, Q^2)$, the nucleon asymmetries $A_{1p,2p}(x, Q^2)$ for the protons as well as the Ellis-Jaffe, Bjorken, Burkhardt-Cottingham and Gottfried sum rule integrals. All the numerical results show good agreement with the experimental data available in the literature. This work may be helpful in understanding the upcoming experimental results from JLab, EIC and CERN collaborations and the role of higher order corrections in the concerned kinematic range of x and Q^2 . We summarize our findings below:

- The perturbative evolution of the polarized parton densities at higher orders in the perturbative expansion is quite important in the determination of polarized nucleon structure functions and the higher order correction terms make significant contributions to the kinematic range of Bjorken x and Q^2 studied in the present work.
- The inclusion of nonperturbative twist-3 correction does not make any significant changes in the evaluation of the polarized nucleon structure functions in the considered range of x and Q^2 . We have also used the kinematic constraint on the center of mass energy $W \geq 2$ GeV, which excludes the region of higher x , where nonperturbative higher order QCD corrections become important.
- We find that the nucleon asymmetries $A_{1p}(x, Q^2)$, $A_{2p}(x, Q^2)$ and the ratios $\frac{g_{1p,1n}(x, Q^2)}{F_{1p,1n}(x, Q^2)}$ increases with the increase in x . However, $A_{2p}(x, Q^2)$ gets saturated after a certain value of x . The inclusion of higher order perturbative and nonperturbative corrections bring the numerical results into better agreement with the experimental data.
- The numerical results for the different sum rule integrals may provide important information about the helicities of quarks, flavor asymmetry of sea quarks, axial and strong coupling constants in the presence of higher order corrections.
- The experimental data with high statistics are required, especially in the region of very low x and high x in order to avoid the uncertainties arising due to the extrapolation of polarized parton densities in the evaluation of the sum rule integrals.

Since future experiments at JLab and EIC at BNL are planned to use the light to heavy nuclear targets such as 2D , 3He , ^{12}C , ^{16}O , ^{56}Fe , etc., therefore, the understanding of nuclear medium effects on the polarized structure functions is important. We plan to study these nuclear medium effects in different nuclear targets by taking into account the nuclear effects due to the Fermi motion and binding energy of the nucleons, the nucleon-nucleon correlations, the shadowing/antishadowing and mesonic cloud contributions in a wide kinematic range of x and Q^2 relevant for future experiments.

Acknowledgment

F. Zaidi is thankful to Council of Scientific & Industrial Research, Govt. of India for providing Senior Research Associateship (SRA) under the Scientist's Pool Scheme, file no. 13(9240-A)2023-POOL and to the Department of Physics, Aligarh Muslim University, Aligarh for providing the necessary facilities to pursue this research work. M. S. A. is thankful to the Department of Science and Technology (DST), Government of India for providing financial assistance under Grant No. SR/MF/PS-01/2016-AMU/G.

[1] J. Ashman *et al.* [European Muon], Phys. Lett. B **206**, 364 (1988).
 [2] R. P. Feynman, Phys. Rev. Lett. **23**, 1415-1417 (1969)
 [3] R. P. Feynman, "Photon-hadron interactions."
 [4] P. L. Anthony *et al.* [E142], Phys. Rev. Lett. **71**, 959-962 (1993).

[5] K. Abe *et al.* [E143], Phys. Rev. D **58**, 112003 (1998).

[6] K. Abe *et al.* [E154], Phys. Rev. Lett. **79**, 26-30 (1997).

[7] P. L. Anthony *et al.* [E155], Phys. Lett. B **458**, 529-535 (1999).

[8] P. L. Anthony *et al.* [E155], Phys. Lett. B **493**, 19-28 (2000).

[9] P. L. Anthony *et al.* [E155], Phys. Lett. B **553**, 18-24 (2003).

[10] B. Adeva *et al.* [Spin Muon (SMC)], Phys. Lett. B **412**, 414-424 (1997).

[11] D. Adams *et al.* [Spin Muon (SMC)], Phys. Rev. D **56**, 5330-5358 (1997).

[12] B. Adeva *et al.* [Spin Muon], Phys. Rev. D **58**, 112001 (1998).

[13] M. G. Alekseev *et al.* [COMPASS], Phys. Lett. B **690**, 466-472 (2010).

[14] C. Adolph *et al.* [COMPASS], Phys. Lett. B **753**, 18-28 (2016).

[15] C. Adolph *et al.* [COMPASS], Phys. Lett. B **769**, 34-41 (2017).

[16] A. Airapetian *et al.* [HERMES], Phys. Lett. B **442**, 484-492 (1998).

[17] A. Airapetian *et al.* [HERMES], Phys. Rev. D **75**, 012007 (2007).

[18] A. Airapetian *et al.* [HERMES], Eur. Phys. J. C **72**, 1921 (2012).

[19] R. Fatemi *et al.* [CLAS], Phys. Rev. Lett. **91**, 222002 (2003).

[20] K. Kramer, D. S. Armstrong, T. D. Averett, W. Bertozi, S. Binet, C. Butuceanu, A. Camsonne, G. D. Cates, J. P. Chen and S. Choi, *et al.* Phys. Rev. Lett. **95**, 142002 (2005).

[21] K. V. Dharmawardane *et al.* [CLAS], Phys. Lett. B **641**, 11-17 (2006).

[22] Y. Prok *et al.* [CLAS], Phys. Rev. C **90**, no.2, 025212 (2014).

[23] A. Deur, Y. Prok, V. Burkert, D. Crabb, F. X. Girod, K. A. Griffioen, N. Guler, S. E. Kuhn and N. Kvaltine, Phys. Rev. D **90**, no.1, 012009 (2014).

[24] G. Altarelli and G. G. Ross, Phys. Lett. B **212**, 391-396 (1988).

[25] M. Anselmino, A. Efremov and E. Leader, Phys. Rept. **261**, 1-124 (1995) [erratum: Phys. Rept. **281**, 399-400 (1997)].

[26] R. D. Ball, S. Forte and G. Ridolfi, Phys. Lett. B **378**, 255-266 (1996).

[27] G. Altarelli, R. D. Ball, S. Forte and G. Ridolfi, Acta Phys. Polon. B **29**, 1145-1173 (1998)

[28] S. D. Bass, Rev. Mod. Phys. **77**, 1257-1302 (2005).

[29] F. Bissey, F. G. Cao and A. I. Signal, Phys. Rev. D **73**, 094008 (2006).

[30] J. D. Bjorken, Phys. Rev. **179**, 1547-1553 (1969).

[31] J. I. Friedman, H. W. Kendall and R. E. Taylor, SLAC-REPRINT-1991-019.

[32] L. W. Whitlow, S. Rock, A. Bodek, E. M. Riordan and S. Dasu, Phys. Lett. B **250**, 193-198 (1990).

[33] M. Arneodo *et al.* [New Muon], Nucl. Phys. B **483**, 3-43 (1997).

[34] A. Airapetian *et al.* [HERMES], JHEP **05**, 126 (2011).

[35] G. Altarelli and G. Parisi, Nucl. Phys. B **126**, 298 (1977);
V. N. Gribov and L. N. Lipatov, Sov. J. Nucl. Phys. **15**, 438 (1972), [Yad. Fiz. **15**, 781 (1972)];
L. N. Lipatov, Sov. J. Nucl. Phys. **20**, 94 (1975), [Yad. Fiz. **20**, 181 (1974)];
Y. L. Dokshitzer, Sov. Phys. JETP **46**, 641 (1977) [Zh. Eksp. Teor. Fiz. **73**, 1216 (1977)].

[36] K. G. Wilson, Phys. Rev. **179**, 1499-1512 (1969).

[37] R. A. Brandt and G. Preparata, Nucl. Phys. B **27**, 541-567 (1971).

[38] N. H. Christ, B. Hasslacher and A. H. Mueller, Phys. Rev. D **6**, 3543 (1972).

[39] I. Borsa, D. de Florian and I. Pedron, Eur. Phys. J. C **82**, no.12, 1167 (2022).

[40] M. Salimi-Amiri, A. Khorramian, H. Abdolmaleki and F. I. Olness, Phys. Rev. D **98**, no.5, 056020 (2018).

[41] H. Khanpour, S. T. Monfared and S. Atashbar Tehrani, Phys. Rev. D **95**, no.7, 074006 (2017).

[42] A. Mirjalili and S. Tehrani Atashbar, Phys. Rev. D **105**, no.7, 074023 (2022).

[43] J. Blumlein and H. Bottcher, Nucl. Phys. B **841**, 205-230 (2010).

[44] E. Leader, A. V. Sidorov and D. B. Stamenov, Phys. Rev. D **73**, 034023 (2006).

[45] J. Blumlein and A. Tkabladze, Nucl. Phys. B **553**, 427-464 (1999).

[46] V. M. Braun, T. Lautenschlager, A. N. Manashov and B. Pirnay, Phys. Rev. D **83**, 094023 (2011).

[47] A. N. Khorramian, S. Atashbar Tehrani, S. Taheri Monfared, F. Arbabifar and F. I. Olness, Phys. Rev. D **83**, 054017 (2011).

[48] D. de Florian, R. Sassot, M. Stratmann and W. Vogelsang, Phys. Rev. Lett. **101**, 072001 (2008).

[49] M. Hirai *et al.* [Asymmetry Analysis], Nucl. Phys. B **813**, 106-122 (2009).

[50] F. Taghavi-Shahri, H. Khanpour, S. Atashbar Tehrani and Z. Alizadeh Yazdi, Phys. Rev. D **93**, no.11, 114024 (2016).

[51] E. R. Nocera *et al.* [NNPDF], Nucl. Phys. B **887**, 276-308 (2014).

[52] E. B. Zijlstra and W. L. van Neerven, Nucl. Phys. B **417**, 61-100 (1994) [erratum: Nucl. Phys. B **426**, 245 (1994); erratum: Nucl. Phys. B **773**, 105-106 (2007); erratum: Nucl. Phys. B **501**, 599-599 (1997)].

[53] W. Vogelsang, Nucl. Phys. B **475**, 47-72 (1996).

[54] J. Blumlein and N. Kochelev, Nucl. Phys. B **498**, 285-309 (1997).

[55] F. Zaidi, H. Haider, M. Sajjad Athar, S. K. Singh and I. Ruiz Simo, Phys. Rev. D **99**, no.9, 093011 (2019).

[56] V. W. Hughes and J. Kuti, Ann. Rev. Nucl. Part. Sci. **33**, 611-644 (1983).

[57] C. A. Aidala, S. D. Bass, D. Hasch and G. K. Mallot, Rev. Mod. Phys. **85**, 655-691 (2013).

[58] R. G. Roberts, Cambridge University Press, 1994, ISBN 978-0-521-44944-1, 978-1-139-24244-8 doi:10.1017/CBO9780511564062.

[59] K. Gottfried: Phys. Rev. Lett. **18** (1967) 1174 .

[60] M. Gell-Mann, Phys. Rev. **125**, 1067-1084 (1962).

- [61] M. Gell-Mann, Physics Physique Fizika **1**, 63-75 (1964).
- [62] R. P. Feynman, M. Gell-Mann and G. Zweig, Phys. Rev. Lett. **13**, 678-680 (1964).
- [63] J. D. Bjorken, Phys. Rev. **148**, 1467-1478 (1966).
- [64] J. D. Bjorken, Phys. Rev. D **1**, 1376-1379 (1970).
- [65] J. R. Ellis and R. L. Jaffe, Phys. Rev. D **9**, 1444 (1974) [erratum: Phys. Rev. D **10**, 1669 (1974)].
- [66] H. Burkhardt and W. N. Cottingham, Annals Phys. **56**, 453-463 (1970).
- [67] S. Wandzura and F. Wilczek, Phys. Lett. B **72**, 195-198 (1977).
- [68] M. S. Athar and S. K. Singh, Cambridge University Press, 2020, ISBN 978-1-108-77383-6, 978-1-108-48906-5 doi:10.1017/9781108489065
- [69] C. G. Callan, Jr. and D. J. Gross, Phys. Rev. Lett. **22**, 156 (1969).
- [70] S. Forte, M. L. Mangano and G. Ridolfi, Nucl. Phys. B **602**, 585-621 (2001).
- [71] W. L. van Neerven and A. Vogt, Nucl. Phys. B **568**, 263 (2000); *ibid* **588**, 345 (2000).
- [72] J. A. M. Vermaseren, A. Vogt and S. Moch, Nucl. Phys. B **724**, 3-182 (2005).
- [73] S. Moch, J. A. M. Vermaseren and A. Vogt, Phys. Lett. B **606**, 123-129 (2005).
- [74] F. Hekhorn, G. Magni, E. R. Nocera, T. R. Rabemananjara, J. Rojo, A. Schaus and R. Stegeman, Eur. Phys. J. C **84**, no.2, 189 (2024).
- [75] S. Stein, W. B. Atwood, E. D. Bloom, R. L. Cottrell, H. C. DeStaebler, C. L. Jordan, H. Piel, C. Y. Prescott, R. Siemann and R. E. Taylor, Phys. Rev. D **12**, 1884 (1975).
- [76] J. J. Aubert *et al.* [European Muon], Phys. Lett. B **123**, 123-126 (1983) doi:10.1016/0370-2693(83)90971-1
- [77] J. J. Aubert *et al.* [European Muon], Nucl. Phys. B **293**, 740-786 (1987).
- [78] A. C. Benvenuti *et al.* [BCDMS], Phys. Lett. B **237**, 599-604 (1990).
- [79] M. Arneodo *et al.* [New Muon], Phys. Rev. D **50**, R1-R3 (1994).
- [80] A. C. Benvenuti *et al.* [BCDMS Collaboration], Phys. Lett. B **223**, 485 (1989); Phys. Lett. B **195**, 91 (1987).
- [81] J. Gomez, R. G. Arnold, P. E. Bosted, C. C. Chang, A. T. Katramatou, G. G. Petratos, A. A. Rahbar and S. E. Rock *et al.*, “Measurement of the A-dependence of deep inelastic electron scattering,” Phys. Rev. D **49**, 4348 (1994).
- [82] M. Arneodo *et al.*, Nucl. Phys. B **481**, 3 (1996).
- [83] J. J. Aubert *et al.* [European Muon Collaboration], Nucl. Phys. B **259**, 189 (1985).
- [84] L. A. Harland-Lang, A. D. Martin, P. Motylinski and R. S. Thorne, Eur. Phys. J. C **75**, no.5, 204 (2015).
- [85] S. E. Kuhn, J. P. Chen and E. Leader, Prog. Part. Nucl. Phys. **63**, 1-50 (2009).